THE ANATOMICAL RECORD PART A 275A:1048–1072 (2003)

Cranial Allometry, Phylogeography, and Systematics of Large-Bodied Papionins (Primates: Cercopithecinae) Inferred From Geometric Morphometric Analysis of Landmark Data

STEPHEN R. FROST,[1]* LESLIE F. MARCUS,[2–4] FRED L. BOOKSTEIN,[5,6] DAVID P. REDDY,[3,7] AND ERIC DELSON[2–4,8]

[1]Department of Anatomy, New York College of Osteopathic Medicine, Old Westbury, New York
[2]Division of Paleontology, American Museum of Natural History, New York, New York
[3]New York Consortium in Evolutionary Primatology (NYCEP) Morphometrics Group, New York, New York
[4]City University of New York Graduate Center, New York, New York
[5]Institute of Anthropology, Vienna, Austria
[6]Institute of Gerontology, University of Michigan, Ann Arbor, Michigan
[7]Library Services, American Museum of Natural History, New York, New York
[8]Department of Anthropology, Lehman College/C.U.N.Y., Bronx, New York

ABSTRACT

The cranial morphology of the African Old World monkeys *Mandrillus*, *Papio*, and *Theropithecus* (i.e., baboons) has been the subject of a number of studies investigating their systematic relationships, patterns of scaling, and growth. In this study, we use landmark-based geometric morphometrics and multivariate analysis to assess the effects of size, sex, taxonomy, and geographic location on cranial shape. Forty-five landmarks were digitized in three dimensions on 452 baboon crania and subjected to generalized Procrustes analysis (GPA), which standardizes geometric size but leaves scaling-based shape differences in the data. The resulting shape coordinates were submitted to regression analysis, principal components analysis (PCA), partial least-squares (PLS) analysis, and various clustering techniques. Scaling (shape differences correlated with size) was the largest single factor explaining cranial shape variation. For instance, most (but not all) of the shape differences between the sexes were explained by size dimorphism. However, central tendencies of shape clearly varied by taxon (both specific and subspecific) even after variations in size and sex were adjusted out. Within *Papio*, about 60% of the size- and sex-adjusted shape variations were explained by the geographic coordinates of the specimen's provenance, revealing a stepped cline in cranial morphology, with the greatest separation between northern and southern populations. Based on evidence from genetic studies, and the presence of at least two major hybrid/interbreeding zones, we interpret the phylogeographic pattern of cranial variation as indicating that these populations are best ranked as subspecies of a single species, rather than as two or more distinct biological species. This objective approach can be applied to other vertebrate species or species groups to help determine the taxonomic rank of problematic taxa. Anat Rec Part A 275A:1048–1072, 2003.

Key words: *Mandrillus*; *Papio*; *Theropithecus*; morphology; Africa; species; subspecies

Grant sponsor: National Science Foundation; Grant number: ACI-9982351; Grant sponsor: CUNY Collaborative Incentive; Grant number: 9-91980; Grant sponsor: Wenner-Gren Foundation; Grant number: 6436; Grant sponsor: L.S.B. Leakey Foundation.

Leslie F. Marcus is deceased.

*Correspondence to: Stephen R. Frost, Department of Anatomy, New York College of Osteopathic Medicine, NYIT, Old Westbury, NY 11568. Fax: (212) 769-5842. E-mail: sfrost@iris.nyit.edu

Received 1 April 2003; Accepted 24 July 2003

DOI 10.1002/ar.a.10112

The large-bodied African cercopithecines *Mandrillus*, *Papio*, and *Theropithecus* were described by Jolly (1970) as an "adaptive array." These taxa do not form a monophyletic clade with respect to the other papionins, but they share a variety of features (e.g., large size, generally long faces, and a high degree of terrestriality) and thus have all been termed "baboons." The morphological and genetic distinctions among these forms, and their phylogenetic relationships have been the subject of many analyses, with conflicting results. Here we apply a geometric morphometrics approach to quantitatively investigate and visualize the patterns of morphological variations of the baboon face in both a phylogenetic and a geographic context.

Several previous authors have studied facial skeletal morphology in papionins by the use of standard distance-based measurements (e.g., Zuckerman, 1926; Freedman, 1962, 1963; Vogel, 1968; Cheverud, 1989; Leigh and Cheverud, 1991). Ravosa and Profant (2000) provided a review of many such studies. These studies, including ontogenetic analyses, documented several of the most important growth and scaling patterns in the papionins. They showed both that features such as facial length and brow ridge projection are positively correlated with size among adults of different species, and that this pattern results from differential extension or accelerated relative growth rates of these features during ontogeny. For example, Freedman (1962, 1963) demonstrated that most of the differences in facial length among baboon subspecies are due to ontogenetic scaling. Albrecht (1978) observed a similar pattern among Sulawesi macaques. Other studies have found differences in scaling patterns among species or larger clades. Fooden (1975, 1988) noted that different species of macaque exhibit divergent scaling patterns. Ravosa and Profant (2000) pointed out that while the overall ontogenetic patterns of macaques and baboons are similar, macaques have relatively shorter faces.

While most of the above analyses focused on scaling patterns within and among species, few have focused on differences in cranial shape other than scaling patterns. A recent landmark-based geometric morphometric study on the face of the mangabey *Cercocebus torquatus* compared facial growth with patterns of bone remodeling, and found that ontogenetic scaling did not account for all of the differences between adult males and females (O'Higgins and Jones, 1998). Those results were in agreement with Enlow's (1975) hypothesis that consistency of remodeling activity indicates consistency of ontogenetic scaling. A geometric morphometric study comparing adult cranial shape and scaling in the Papionini used the same data collection protocol as used in the present study, and included some of the same specimens (Singleton, 2002). In that analysis, patterns of adult scaling were shown to differ among the papionins: *Macaca*, *Papio*, and *Mandrillus* shared one common allometric pattern, while the mangabeys *Lophocebus* and *Cercocebus* shared a second pattern. However, it was found that after the effects of scaling were taken into account, there were clear differences among all genera in cranial shape, including between both of the mangabey genera and between *Papio* and *Mandrillus*. Collard and O'Higgins (2001) analyzed the same genera, but included juvenile specimens in their samples. Unfortunately, they lacked sufficient *Theropithecus* specimens to include them in the analysis. They described differences in ontogenetic scaling between *Papio* and *Mandrillus*, and between *Cercocebus* and *Lophocebus*. Both of these studies generally analyzed only a single (sub)species within each genus, and both studies chose different species for most genera. This could potentially lead to important differences between these studies and others, depending on which species are included. Within *Macaca*, for instance, there is considerable diversity of cranial form (e.g., Albrecht, 1978), and within *Papio* there are some differences in adult scaling patterns between subspecies.

Baboons take on an added importance because they have been used as models for early human distribution, behavioral adaptation, and systematic patterns since the work of DeVore and Washburn (1963) (see also Jolly, 1972, 2001). As widespread, terrestrial, and relatively large-bodied African catarrhines, *Papio* may represent a better analogue for australopiths (and perhaps also early *Homo*) in terms of ecology and phylogeography than do the far more closely related great apes. The same problems of taxonomy and morphological variation have perplexed students of both early human and baboon systematics.

BABOON SYSTEMATICS

Despite over two centuries of study, the taxonomy of the baboons, and the relationships among them, remain controversial. *Papio*, known colloquially as the open-country or savannah baboon (although some live in the forest or desert), has the widest distribution and greatest diversity, but is the least definitively understood in terms of alpha taxonomy. *Mandrillus*, the forest baboon, is comprised of two species restricted to the rain forests of western central Africa. *Theropithecus*, the gelada baboon, is usually considered to include only one extant species, which is restricted in its modern distribution to the grasslands of the Ethiopian highlands. Below we discuss each of these genera and their included variants in order to provide sufficient background for this analysis.

The allopatric mandrills (*Mandrillus sphinx*) and drills (*M. leucophaeus*) are almost always considered as distinct species (e.g., Szalay and Delson, 1979; Napier, 1981; Groves, 1989, 2001; Oates, 1996; Fleagle, 1999). They are found in western central Africa, north and south of the Sanaga River, respectively (Fig. 1). They are similar to the savanna baboons in overall cranial appearance, in that they have a relatively long muzzle, but they also have some unique specializations, such as greatly inflated maxillary ridges in socially dominant adult males (e.g., Szalay and Delson, 1979; Fleagle and McGraw, 1999, 2002). No extinct representatives are yet known. Many morphological analyses have considered *Mandrillus* to be more closely related to *Papio* than is *Theropithecus*, which is often placed as a subgenus within *Papio* (e.g., Jolly, 1967; Hill, 1970; Szalay and Delson, 1979; Strasser and Delson, 1987; Delson and Dean, 1993). However, molecular studies have long argued for a sister-taxon relationship between *Theropithecus* and *Papio* to the exclusion of *Mandrillus*, which has been grouped with *Cercocebus* (Hewett-Emmett et al., 1976; Sarich and Cronin, 1976; Disotell, 1994; Harris and Disotell, 1998; Harris, 2000). Fleagle and McGraw (1999, 2002) also discussed some morphological features that argued for a sister relationship between *Mandrillus* and *Cercocebus*, as well as between *Papio* and *Theropithecus*. Thus, the two widely accepted groupings of African papionins, the larger baboons (*Papio*, *Mandrillus*

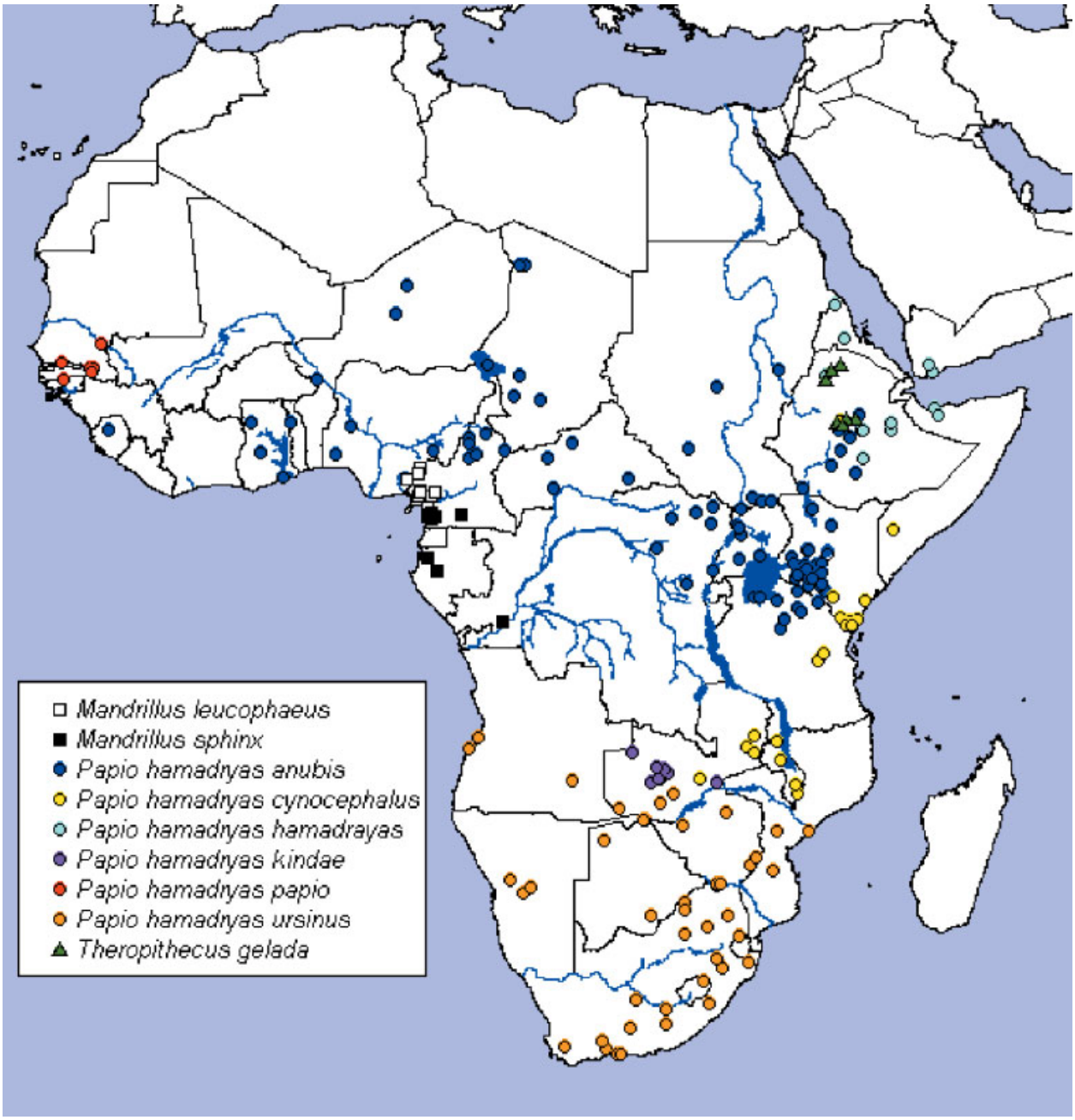

Fig. 1. Map of Africa showing the approximate collecting localities for all individuals with analyzed crania for which geographic data are available. Localities may contain one or more individuals.

and *Theropithecus*), and the smaller mangabeys (*Cercocebus* and *Lophocebus*) are both paraphyletic assemblages.

All modern authors recognize a single extant species within *Theropithecus*: *T. gelada*. Although fossil species of *Theropithecus* are known throughout Africa (as well as in India and Spain), the extant gelada is restricted to the highlands of Ethiopia, both north and south of the Ethiopian Rift Valley (Fig. 1). Populations from south of the rift valley are sometimes recognized as the separate subspecies *T. g. obscurus* (e.g., Hill, 1970). Geladas are unique in many aspects of their biology, including the fact that they are the only extant primate with a diet primarily composed of grass parts (e.g., see Iwamoto, 1993). This dietary specialization may be responsible for their highly distinctive craniofacial morphology (Jolly, 1972; Szalay and Delson, 1979; Delson and Dean, 1993).

In contrast to *Mandrillus* and *Theropithecus*, *Papio* extends in a nearly continuous range from Senegal in the west to Ethiopia and Somalia in the east (and onto the Arabian peninsula), south to the Cape of Good Hope, and west again into Angola (and Zambia). As reviewed most recently by Jolly (1993), extant *Papio* may be interpreted

TABLE 1. Number of specimens by sex for each of the taxa studied in this analysis

Taxon	Females	Males	Both
Mandrillus leucophaeus	11	20	31
Mandrillus sphinx	11	15	26
Papio hamadryas anubis	40	88	128
Papio hamadryas cynocephalus	9	19	28
Papio hamadryas hamadryas	2	21	23
Papio hamadryas kindae	7	8	15
Papio hamadryas papio	1	15	16
Papio hamadryas ursinus	68	87	155
Theropithecus gelada	9	21	30
Totals	158	294	452

as including as many as five morpho-typological species (e.g., Hill, 1970; Napier, 1981; Oates, 1996; Wildman, 2000; Groves, 2001), two species distinguished especially by socioecology (e.g., Thorington and Groves, 1970), or a single species with numerous subspecies and hybrid intergrade zones (e.g., Jolly and Brett, 1973; Szalay and Delson, 1979; Jolly, 1993; Sarmiento, 1999; Delson et al., 2000). For the current work, a single extant biological species is recognized in the genus, with six named subspecies: *P. hamadryas hamadryas*, *P.h. papio*, *P.h. anubis*, *P.h. cynocephalus*, *P.h. kindae*, and *P.h. ursinus*. There is also a considerable amount of morphological and body size variation within some of these subspecies, particularly *P.h. anubis* and *P.h. ursinus*. Jolly (1993) has noted that if these subspecies are recognized, it may be necessary (i.e., equally valid) to accept several others as well. The six subspecies of *Papio* recognized here are distributed across sub-Saharan Africa and Arabia, as shown in Figure 1. Additional species (and perhaps subspecies of *P. hamadryas*) are known in the fossil record, some of which are often placed in the subgenus *P.* (*Dinopithecus*) (see Delson and Dean, 1993).

MATERIALS AND METHODS

Sample

A total of 633 extant baboon crania were digitized by S.F. between 1997 and 1999 at institutions in North America, Europe, and Africa (see Acknowledgments for a comprehensive list). This sample includes specimens of *Theropithecus gelada,* both species of *Mandrillus,* and all six of the recognized extant subspecies of *Papio hamadryas*. Of this total, 452 specimens preserved all of the landmarks used here. Only these complete specimens were used in this analysis. The numbers of specimens for each taxon are presented by sex in Table 1. Sample sizes for the different subspecies are far from equal, but all four species, and all six subspecies of *P. hamadryas* are represented. While the sample is not evenly distributed geographically, it does cover nearly the entire geographic range of all of the included species and subspecies. The sample localities of all specimens included in this analysis (when known) are shown in Figure 1.

Data Collection Protocol

For each specimen, 45 standard craniometric landmarks were recorded in the form of three-dimensional (3D) coordinate data. The landmarks used are shown in Figure 2 and listed in Table 2. Twenty-nine of the landmarks were collected from the dorsal aspect of the cranium while it was mounted in approximately the Frankfurt Horizontal. Sixteen of the landmarks were collected from the ventral aspect of the cranium while it was mounted approximately in norma basilis. Orientations of the specimens were chosen for convenience during data collection and file manipulation, and did not affect subsequent analyses, as all specimens were recentered and rotated. Additionally, four registration points (see below) were marked on each specimen with reusable adhesive and recorded in both orientations. The four registration points were chosen in the form of a large asymmetric tetrahedron, so that the device error would be minimized relative to the size of the tetrahedron.

The data were collected using a Microscribe-3DX 3D multi-joint-arm digitizer (Immersion Corp., San Jose, CA) fitted with a narrow stylus. This device had a precision of approximately 0.26 mm, including human error, in landmark location (Marcus et al., 1997) when applied to the more repeatable landmarks in this study. As mentioned above, all of the data included in this study were collected by a single individual. To estimate the overall precision for this study, S.F. measured two specimens eight times each. Overall precision across all coordinates was 0.36 mm. Precision for type 1 landmarks was generally <0.33 mm. The most variable landmark (the left postglenoid, a type 2 landmark) had a precision of only 1.26 mm, but this is still small relative to the overall size of the baboon skulls. Singleton (2002) found a similar level of error in her study for within-observer precision, using the same data collection protocol and device. Coordinates were recorded directly into Microsoft Excel onto a formatted template. This allowed some screening of the data during digitization, as well as re-collection of erroneous values.

Data collected in the ventral position were aligned together onto the same coordinate system as those collected in the dorsal position by applying a least-squares superimposition of the four ventral orientation points onto the four dorsal points. The rigid rotation derived from the orientation points was then applied to the landmark coordinates. This was done using software written in Practical Extraction and Reporting Language (Perl), with matrix computation done using Matlab 5.0. (For further information regarding least-squares superimposition of coordinate data, see Rohlf and Slice (1990).)

Analytical Methods

Procrustes analysis. The data set used in this analysis contained 135 coordinates for the 45 landmarks for all 452 specimens. A generalized Procrustes analysis (GPA) superimposition was performed using the TPS Small software package (Rohlf, 2002). Centroid size was computed for each specimen at the same time. Centroid size is computed as the square root of the sum of squared distances of a set of landmarks from their centroid. Any analysis using GPA-superimposed coordinates faces the problem that the data are in a non-Euclidean shape space (Rohlf, 1999). The data are then projected into a Euclidean space tangent to this shape space for statistical analysis (Dryden and Mardia, 1998; Rohlf, 1999); here these will be termed "tangent space coordinates." For this analysis, GPA-aligned coordinates were projected into tangent space using the "orthogonal" option of TPS Small, which is the preferred method (Rohlf, 1999). If shape variation in the sample is small enough, then tangent space will provide an acceptable approximation to Procrustes shape space

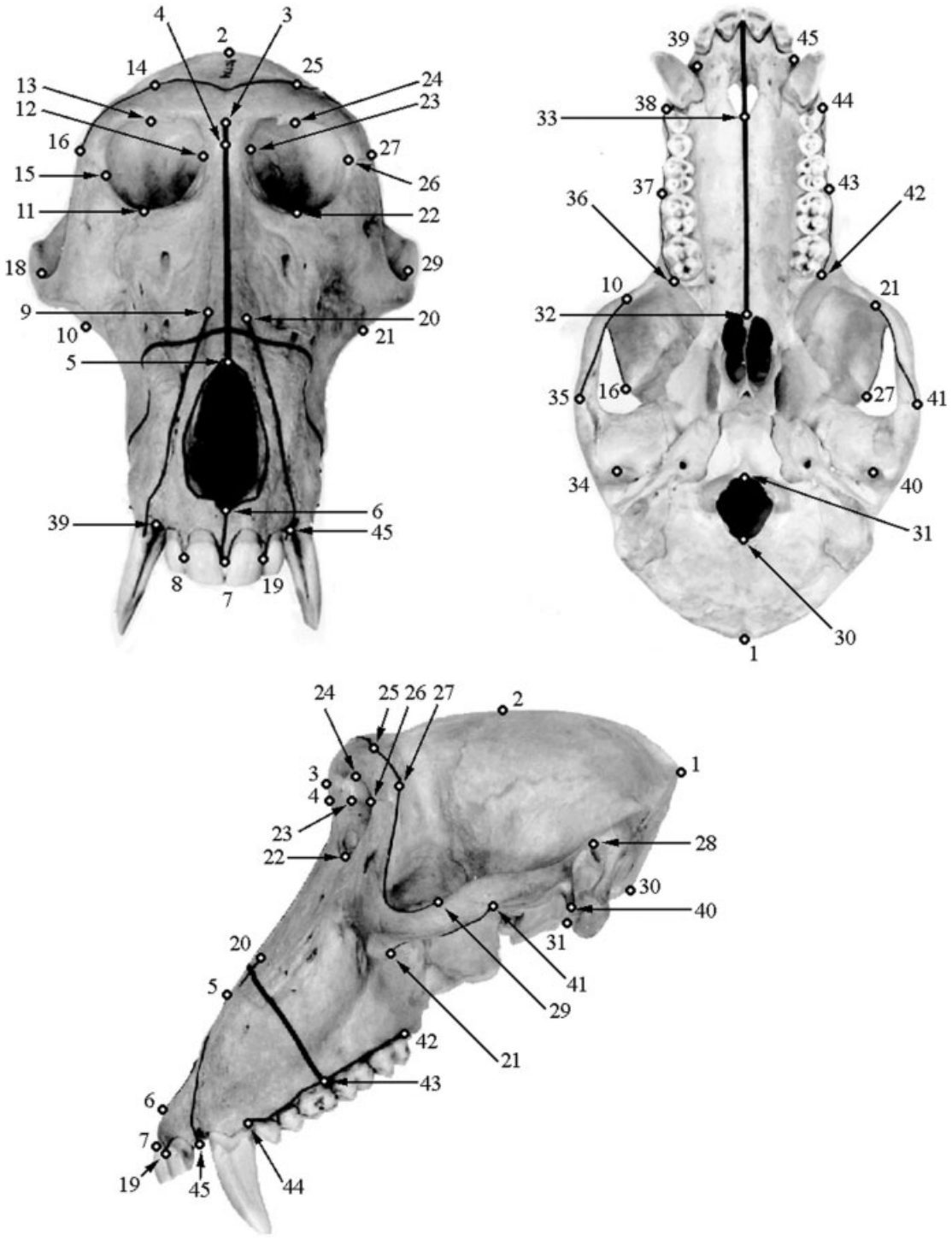

Fig. 2. Baboon (*Papio hamadryas ursinus* male) cranium with landmarks and space curves collected. The landmarks are indicated by dots and labeled with numbers that correspond to those in Table 2.

(Dryden and Mardia, 1998; Rohlf, 1999). To verify that the difference between tangent space and shape space was minimal, interspecimen tangent distances were regressed on Procrustes distances using TPS Small. The resultant uncentered correlation of 0.999999 and root mean square error of 0.000014 indicated that these two spaces were nearly identical for the data set used here. Tangent space coordinates and centroid sizes were exported from TPS Small and analyzed using the SAS system 8.00 for Windows (SAS Institute, Cary, NC).

TABLE 2. Landmarks collected for all specimens*

No.	Point	SF	W00	Definition
Midline				
1.	Inion	IN	i	Most posterior point of cranium, when viewed in the Frankfurt horizontal, be it on sagittal/nuchal crest or not.
2.	Bregma	BR	b	Junction of coronal and sagittal sutures, on sagittal crest if necessary.
3.	Glabella	GL	g	As viewed in Frankfurt horizontal.
4.	Nasion	NA	n	Fronto-nasal suture in midline.
5.	Rhinion	RH	rhi	Most anterior point in midline on nasals.
6.	Nasospinale	NS	ns	Inferiormost midline point of piriform aperture.
7.	Prosthion	PR	pr	Anteroinferior point on projection of premaxilla between central incisors.
30.*	Opisthion	OP	o	Posterior most point of foramen magnum.
31.	Basion	BA	ba	Anterior most point of foramen magnum.
32.	Staphylion	ST	sta	Midline point on palate on line tangent to anterior most points on choanae.
33.	Incisivion	IV		Midline point at the anterior most point of the maxilla (=posterior end of the incisive foramen), extrapolated if broken or asymmetrical.
Bilateral (right/left)				
8./19.	Prosthion2	PR2		Antero-inferiormost point on pre maxilla, equivalent to prosthion, but between central and lateral incisors.
9./20.	Premax-max superior	PMS		Where premaxillo-maxillary suture meets nasal bone, or aperture, if it does not continue to the nasal bone.
10./21.	Zygo-max inferior	ZMI		Anteroinferior point of zygomaticomaxillary suture, in antero-lateral view.
11./22.	Zygo-max superior	ZMU		Anterosuperior point of zygomaticomaxillary suture (taken at orbit rim).
12./23.	Dacryon	DAC	d	Junction of frontal, lacrimal and maxilla.
13./24.	Mid-torus inferior	MTI		Point on inferior margin of supraorbital torus (superior margin of orbit) roughly at middle of orbit.
14./25.	Mid-torus superior	MTS		Superior to MTI on superior most point of supraorbital torus when viewed in Frankfurt horizontal (see Line I).
15./26.	Frontomalare orbitale	FMO	fmo	Where frontozygomatic suture crosses the inner orbital rim.
16./27.	Frontomalare temporale	FMT	fmt	Where frontozygomatic suture crosses lateral edge of zygoma (LEZ) if suture isn't straight, project course of middle third laterally to LEZ.
17./28.	Porion	PO	po	(In Frankfurt horizontal--defines) top of auditory meatus.
18./29.	Zygo-temp superior	ZTS		Superior point of zygomatico-temporal suture on lateral face of zygomatic arch.
34./40.	Postglenoid	PG		Tip (or midpoint of area).
35./41.	Zygo-temp inf	ZTI		Inferolateral point of zygomaticotemporal suture on lateral face of zygomatic arch.
36./42.	Distal M3	M3D		Distal midpoint projected (laterally) onto alveolar margin.
37./43.	M1–2 contact	M12		Projected (laterally) onto alveolar margin.
38./44.	Mesial P3	MP3		Most mesial point on P3 alveolus, projected onto alveolar margin.
39./45.	Premax-max inf	PMI		Where premaxillomaxillary suture crosses alveolar margin.

*The number corresponds to the order in which they are collected, and matches those of Figure 2. Landmark abbreviations in the SF column are those used here. Those in the W00 column are the equivalents in White (2000).
Landmarks numbered 30 and higher are collected in the ventral orientation, all others are collected in the dorsal orientation.

To compare differences in shape among groups, mean configurations were computed for each genus and for each (sub)species, and Procrustes distances were computed between these means, both on the tangent space coordinates, and after adjusting them for size and sex (see below). Procrustes distances among (sub)species are shown in Table 3. In the formula used here, the squared Procrustes distance is the minimum summed squared distance between the landmarks of two size-standardized landmark configurations (other formulas have been used (e.g., Dryden and Mardia, 1998)). Thus, sums of squares among these tangent space coordinates measure explained shape variation among the landmark configurations.

Regression analysis. To examine the effects of various factors on shape, a series of multivariate multiple least-squares linear regression analyses were performed on the 135 tangent space coordinates, with various factors as the independent variables, including size, sex, and taxon. Regression analyses for sex and taxon were performed by coding these factors as "dummy" variables (e.g., coding *Mandrillus* as "1" and Papio and *Theropithecus* as

TABLE 3. Two measures of shape difference between (sub)species*

	Mlc	Msp	Pha	Phc	Phh	Phk	Php	Phu	Tgl
Mlc	–	0.0428	0.0740	0.0985	0.0841	0.1051	0.0859	0.1000	0.1293
Msp	0.00183	–	0.0657	0.0862	0.0707	0.0907	0.0793	0.0865	0.1155
Pha	0.00549	0.00432	–	0.0369	0.0274	0.0488	0.0369	0.0397	0.0886
Phc	0.00974	0.00745	0.00135	–	0.0415	0.0335	0.0474	0.0235	0.0950
Phh	0.00709	0.00501	0.00074	0.00172	–	0.0569	0.0407	0.0407	0.0857
Phk	0.01108	0.00825	0.00238	0.00112	0.00324	–	0.0577	0.0414	0.1086
Php	0.00740	0.00630	0.00136	0.00225	0.00165	0.00332	–	0.0490	0.1054
Phu	0.01003	0.00750	0.00157	0.00055	0.00165	0.00171	0.00240	–	0.0846
Tgl	0.01681	0.01340	0.00788	0.00905	0.00737	0.01183	0.01115	0.00718	–

*Procrustes distance between size and sex adjusted means are tabulated above the diagonal. Below the diagonal are presented Euclidean distances among centroids for each taxon based on size and sex adjusted PCA.

"0"). Coefficients from these regressions are vectors representing the change in shape correlated with the independent variable. These vectors are referred to as "regressions" (e.g., size regression, sex regression, mandrill regression, etc.). Sums of squares among the residuals from these regressions measure residual shape variation among landmark configurations after adjusting for the independent variable. When we report the fraction of shape variance explained by various factors, it is from regressions of shape on these variables. The explained Procrustes sums of squares are all shown in Table 4.

While differences in geometric scale were removed during the GPA, aspects of shape variation correlated with size (in other words allometric components of shape) were not. Previous morphometric analyses have shown that there is a large component of shape variation that is correlated with size in papionins (e.g., Freedman, 1962, 1963; Ravosa and Profant, 2000; Collard and O'Higgins, 2001; Singleton, 2002). To examine this, tangent space coordinates were regressed against the natural log of centroid size. Centroid size has been shown to be a convenient estimator for size in geometric morphometric analyses (Bookstein, 1996; Slice et al., 1996). Furthermore, it is highly correlated with body mass for the taxa included in this analysis ($R^2 = 0.94$ on natural log-transformed, sex-specific species mean body mass data from Delson et al. (2000) (for all species and subspecies used here except *M. leucophaeus* and *P.h. papio*, which lacked mass data); see Fig. 3). Centroid size explains 35% of the total shape variation in the data set. Sex by itself accounts for 18%, and size and sex together account for 39%. Residuals from each of these three regressions were assembled and used as "size-adjusted," "sex-adjusted," or "size- and sex-adjusted" data sets.

Principal component analysis (PCA). PCA rotates the data so that they are represented by a new matrix of full rank, with each of the vectors being uncorrelated, and ordinated in terms of amount of variance explained (Neff and Marcus, 1980; Manly, 1994). The principal components of tangent space coordinates are interpreted as dimensions that explain relatively large amounts of shape variation. In any such PCA, there are seven dimensions of exactly zero explained variance, corresponding to the normalizations in the course of the Procrustes fit operations (three due to translation along three axes, three due to rotation about three axes, and one due to scale adjustment). Any asymmetries of the actual landmark data set are preserved by these PCAs. Several PCAs were performed in this study, all of which were computed using the covariance matrix of tangent space coordinates or their residuals after regression of size and sex. Similar PCAs were also computed within each of the genera. The eigenvalues of the first five PCs of these are also reported in Table 5.

One PCA was performed on the covariance matrix of the tangent space coordinates of the whole sample. The proportion of the total variance for each principal component and the cumulative total for the first five principal components from this PCA are given in Table 5. The first

TABLE 4. Proportion of total procrustes distance accounted for by different factors

Factor	Procrustes sum of squares	Percentage of total (%)
Total sample		
Total	0.00802	100.0
ln(centsize)	0.00281	35.1
Sex	0.00145	18.1
ln(centsize) & sex	0.00311	38.9
Mandrill	0.000730	9.1
Gelada	0.000893	11.1
Genus	0.00163	20.4
ln(centsize) & sex & taxon	0.00435	54.3
Mandrillus only		
Total	0.00833	100.0
ln(centsize) & sex	0.00352	42.3
Sex	0.00327	39.3
ln(centsize) & sex	0.00371	44.6
Species	0.000490	5.9
ln(centsize) & sex & taxon	0.00415	49.9
Papio only		
Total	0.00632	100.0
ln(centsize)	0.00267	42.3
Sex	0.00135	21.4
ln(centsize) & sex	0.00290	45.9
P. h. anubis	0.000262	4.2
P. h. cynocephalus	0.0000423	0.7
P. h. hamadryas	0.000181	2.9
P. h. kindae	0.000784	12.4
P. h. papio	0.000152	2.4
Subspecies	0.00164	25.9
ln(centsize) & sex & taxon	0.00285	54.8
Theropithecus only		
Total	0.00393	100.0
ln(centsize)	0.00138	35.0
Sex	0.00121	30.1
ln(centsize) & sex	0.00152	38.8

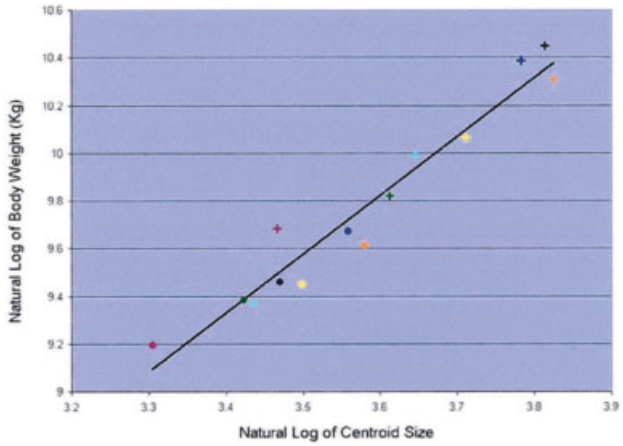

Fig. 3. Bivariate plot with sex-specific taxon mean centroid size on the X-axis, and body mass on the Y-axis. The mean body mass data by sex were obtained from Delson et al. (2000). For *M. sphinx* we used founder population data from Setchel et al. (2001). Plus signs represent males, and circles represent females. Colors are the same as in Figure 1.

TABLE 5. The first five eigenvalues of the covariance matrix on tangent space coordinates for several of the PCAs performed in this analysis

Rank	Eigenvalue	Difference	Proportion	Cumulative
Unadjusted tangent space coordinates				
1	0.00329814	0.00186005	0.4115	0.4115
2	0.00143809	0.00075522	0.1794	0.5909
3	0.00068287	0.00035201	0.0852	0.6761
4	0.00033086	0.00008944	0.0413	0.7173
5	0.00024142	0.00007009	0.0301	0.7475
Size and sex adjusted tangent space coordinates				
1	0.00139893	0.00065799	0.2854	0.2854
2	0.00074094	0.00037457	0.1512	0.4366
3	0.00036637	0.00008503	0.0748	0.5114
4	0.00028133	0.00004547	0.0574	0.5688
5	0.00023586	0.00010013	0.0277	0.6169
Mandrillus tangent space coordinates				
1	0.00373632	0.00202587	0.4487	0.4487
2	0.00171045	0.00115822	0.2054	0.6542
3	0.00055223	0.00025939	0.0663	0.7205
4	0.00029284	0.00006453	0.0352	0.7557
5	0.00022831	0.00004951	0.0274	0.7831
Papio tangent space coordinates				
1	0.00302991	0.00223029	0.4797	0.4797
2	0.00079962	0.00050714	0.1266	0.6063
3	0.00029248	0.00003819	0.0463	0.6527
4	0.00025429	0.00008508	0.0403	0.6929
5	0.00016922	0.00004165	0.0268	0.7197
Theropithecus tangent space coordinates				
1	0.00151980	0.00111834	0.3872	0.3872
2	0.00040146	0.00006064	0.1023	0.4895
3	0.00034082	0.00011218	0.0868	0.5763
4	0.00022864	0.00001964	0.0582	0.6345
5	0.00020900	0.00005434	0.0532	0.6878

principal component from this analysis makes an angle of 12° (cosine 0.98) with the allometry vector from the natural logged centroid size regression.

The residuals from the size-adjusted, sex-adjusted, and size- and sex-adjusted data sets were used for PCAs of their own. Eigenvalues of the five eigenvectors of the covariance matrix from the size- and sex-adjusted data are given in Table 5. Such analyses are preferable to a canonical variates analysis, which goes beyond adjusting for known factors like these to normalize the variance of tiny shape factors, such as fluctuating asymmetry. That sort of normalization is inappropriate in systematic studies (Bookstein, 1996). PCAs of size- and sex-adjusted data for *Papio* were computed for the partial least-squares (PLS) analysis (described below).

Multivariate analysis of covariance (MANCOVA). In order to examine the relationship between shape and size across the various forms of baboons, a MANCOVA was performed. The scores of the first five principal components from the PCA on the unadjusted tangent space coordinates were used as the dependent variables to represent shape, as sample size was insufficient to use the tangent space coordinates themselves. Centroid size, transformed into natural logarithms, was used as the covariate, with taxon and sex as independent variables. First, separate analyses were run within each of the genera to determine whether scaling patterns were consistent internally. Genera were analyzed in a separate analysis. Significant interaction components between taxon and size, or taxon and shape represent differences of scaling pattern, and differences among taxa or sexes represent differences in size-adjusted shape. *P*-values from Wilks' lambda for differences in scaling patterns among subspecies of *Papio hamadryas* are reported in Table 6.

PLS analysis. The first five principal component scores from an analysis of the size- and sex-adjusted *Papio* data were used in a PLS analysis of phylogeography. In the present application, the PLS analysis results in dimensions of shape (that is, linear combinations of shape coordinates) that have the highest covariances with dimensions of "geographic origin" (which means, essentially, lines on a map of Africa). These dimensions are computed by singular-value decomposition of the covariance matrix between all 135 shape coordinates and the two map coordinates, latitude and longitude, for the specimen's point of origin. The analysis was restricted to the 243 crania that had associated locality information. For an introduction to PLS in the more general context of morphometric studies, see Rohlf and Corti (2000).

Matrix multiple regression. To examine the additional contribution to Procrustes distance due to subspecific differences, a matrix multiple regression of shape distance on geographic distance and taxon was performed. Geographically adjacent subspecies were contrasted to see if there was a component of Procrustes distance in addition to that accounted for by geographic distance, due to crossing a subspecific barrier. In this model, the slope of the regression represents the average change in shape per unit of distance (in this case, 1° of latitude or longitude), and the difference in intercept between subspecies represents the additional shape difference due to subspecies difference. Results for the five adjacent subspecies boundaries are given in Table 7.

TABLE 6. Results from MANCOVA of size, sex, and subspecies on shape in *Papio hamadryas*

	Pha	Phc	Phh	Phk	Php	Phu
Pha	–	0.2551	0.3685	0.4381	0.0134	<.0001
Phc	<.0001	–	0.2590	0.1756	0.1362	0.0892
Phh	<.0001	<.0001	–	0.3612	0.0257	0.0461
Phk	<.0001	0.0102	0.0164	–	0.0191	0.7402
Php	<.0001	<.0001	<.0001	<.0001	–	0.0415
Phu	<.0001	<.0001	<.0001	<.0001	<.0001	–

Above the diagonal, *P* values from Wilks' lambda are reported for differences in scaling pattern among subspecies of *Papio hamadryas.* Below the diagonal are *P* values for differences in mean size-adjusted shape. With full Bonferroni adjustment and overall alpha of .05, a *P* value of 0.003 is required for significance.

TABLE 7. Results of matrix multiple regression of shape distance on geographic distance

Comparison	Geography	*P*	Subspecies	*P*	Procrustes distance/1°
P. h. anubis vs. *P. h. cynocephalus*	0.0001	0.0000	0.0094	0.0000	0.000057
P. h. anubis vs. *P. h. hamadryas*	0.0001	0.0000	0.0067	0.0000	0.000057
P. h. anubis vs. *P. h. papio*	0.0001	0.0000	0.0020	0.0000	0.000067
P. h. cynocephalus vs. *P. h. kindae*	0.0003	0.0000	0.0010	0.2165	0.000251
P. h. cynocephalus vs. *P. h. ursinus*	0.0002	0.0000	0.0031	0.0000	0.000172

Geography column represents component of shape difference due to the geographic separation between groups. The subspecies column represents the component of shape difference due to subspecies difference. The Procrustes distance/1° column shows the amount of procrustes distance per 1° of geographic distance.

Visualization. For visualization purposes, and to better elucidate the shape changes associated with the different PCA axes, the eigenvectors were extracted from SAS and were added to and subtracted from the consensus landmark configuration. This allowed us to visualize shape differences implied by extreme values along these vectors. A similar operation was performed with the vector coefficients from the regressions, as well as the vectors produced by the PLS analysis. Two-dimensional (2D) views of 3D thin-plate splines were also computed for different multivariate vectors and the Procrustes regression coefficients. Creases in the thin-plate spline reveal localized areas of shape change (Bookstein, 2000).

RESULTS

Regression Analysis and Differences in Mean Shape

Allometric scaling accounted for the largest proportion (35%) of overall cranial shape variation in the sample (Table 4). The shape changes indicated by allometric scaling (Fig. 4) are generally the same as those described by previous authors. The larger specimens have a relatively longer rostrum, a relatively smaller neurocranium, and a narrower cranium overall compared to the smaller specimens. Furthermore, the posterior part of the rostrum is deeper compared to the zygomatic arch, and the anterior portion of the rostrum is more inferiorly flexed, yielding a palate that slopes more antero-inferiorly. The orbits are smaller and positioned more superiorly on the face. There is a distinct crease (Bookstein, 2000, 2002) in the thin-plate spline near the midpoint of the nasal aperture in the midline, which represents a local maximum of scaling in the direction along the facial plane at this locus. At the maximum, scaling is at a rate of 1.55 times geometric scaling (referred to as the centroid size; Fig. 5).

With the use of size-adjusted data sets, the mean configurations for males and females were visualized. Sex alone accounted for 18% of the total Procrustes sums of squares, but only 3% of the residual variation in the size-adjusted data (Table 4). The two vectors make an angle of 17° (cosine 0.95). Males exhibit a relatively large distance between the landmarks around the canine, and a more upturned premaxilla. Males have relatively flatter and broader supraorbital arches, which are positioned more anteriorly on the cranium. The inion is positioned more superiorly in males (Figs. 6 and 7).

Differences in shape among genera are pronounced after the effects of size and sex are adjusted for, and explain the largest amount of Procrustes sums of squares after scaling (Table 4; Figs. 8–11). Shape differences among genera agree well with those of published descriptions (e.g., Jolly, 1967; Szalay and Delson, 1979; Eck and Jablonski, 1987). Procrustes distances between size and sex-adjusted (sub)species means reveal that the distances among genera are far greater than those among species of *Mandrillus* or subspecies of *Papio* (Table 3). The crania of *Mandrillus* are generally lower and broader than those of *Papio* (Fig. 8). They have a more upturned alveolar plane, longer nasals, and lower glabella, yielding a straighter rostrum and more airorhynchous cranium. The brow ridges are flatter and less arched, and the inion is positioned superior to that of *Papio*. There are distinct creases in the spline between *Papio* and *Mandrillus* size- and sex-adjusted means (Fig. 9). One is on the lateral margins of the neurocranium and brow ridges, related to the narrow overall vault and flattened brows. Another is in the rostrum and palate. *Theropithecus* differs from the other genera in having a superoinferiorly deeper face, particularly under the molars, and a more concave profile in lateral view. The nasals are shorter and the subnasal

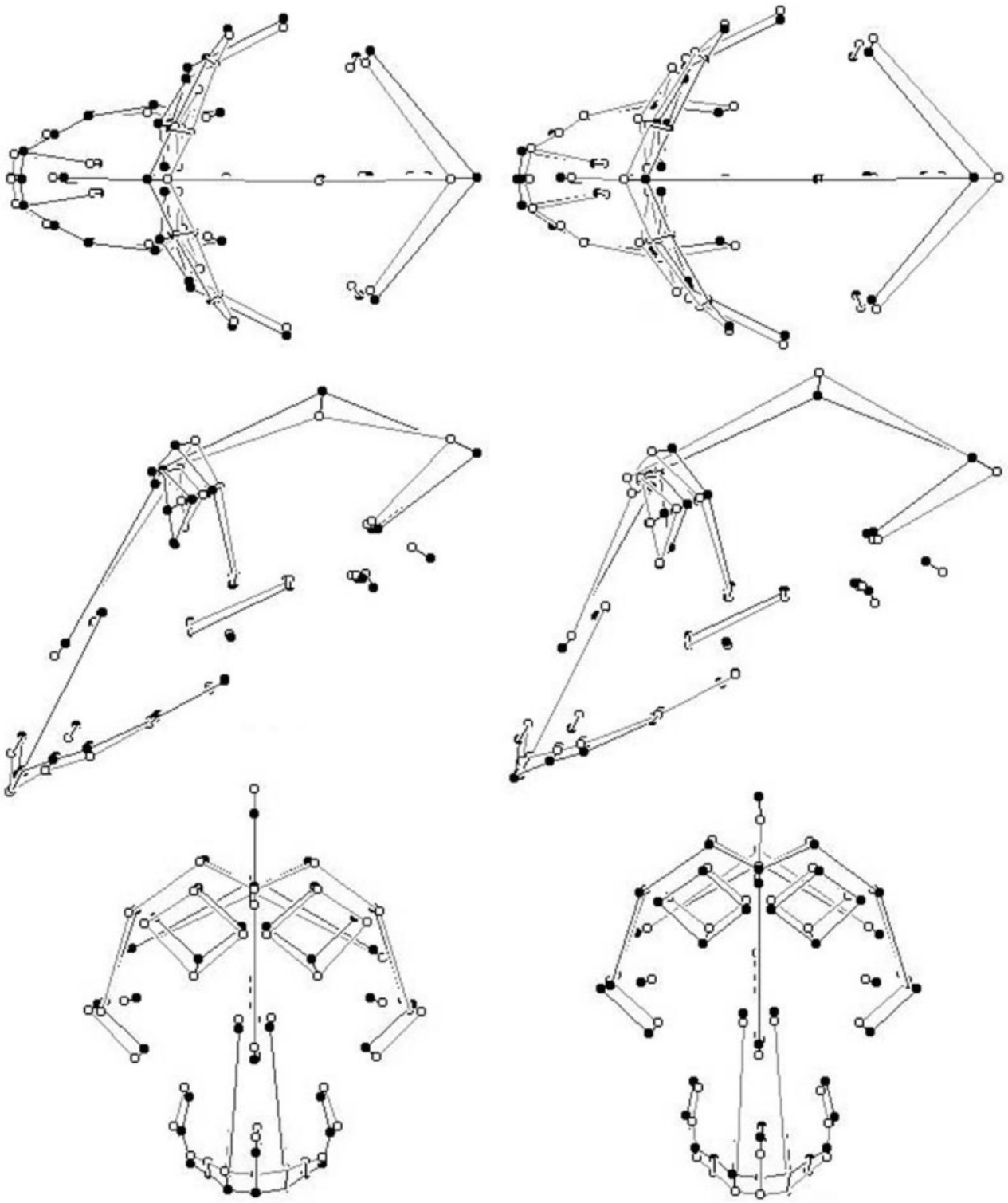

Fig. 4. Visualization of shape changes associated with size in the baboon cranium. Top row: dorsal; middle row: left lateral; bottom row: frontal views of consensus landmark configuration (open circles) and size-related landmark deviations (solid circles), all aligned in Frankfurt horizontal. The left column shows deviations associated with smaller centroid size (solid circles), and the right column shows deviations associated with large size (solid circles). Links connecting landmarks are simply to aid visualization.

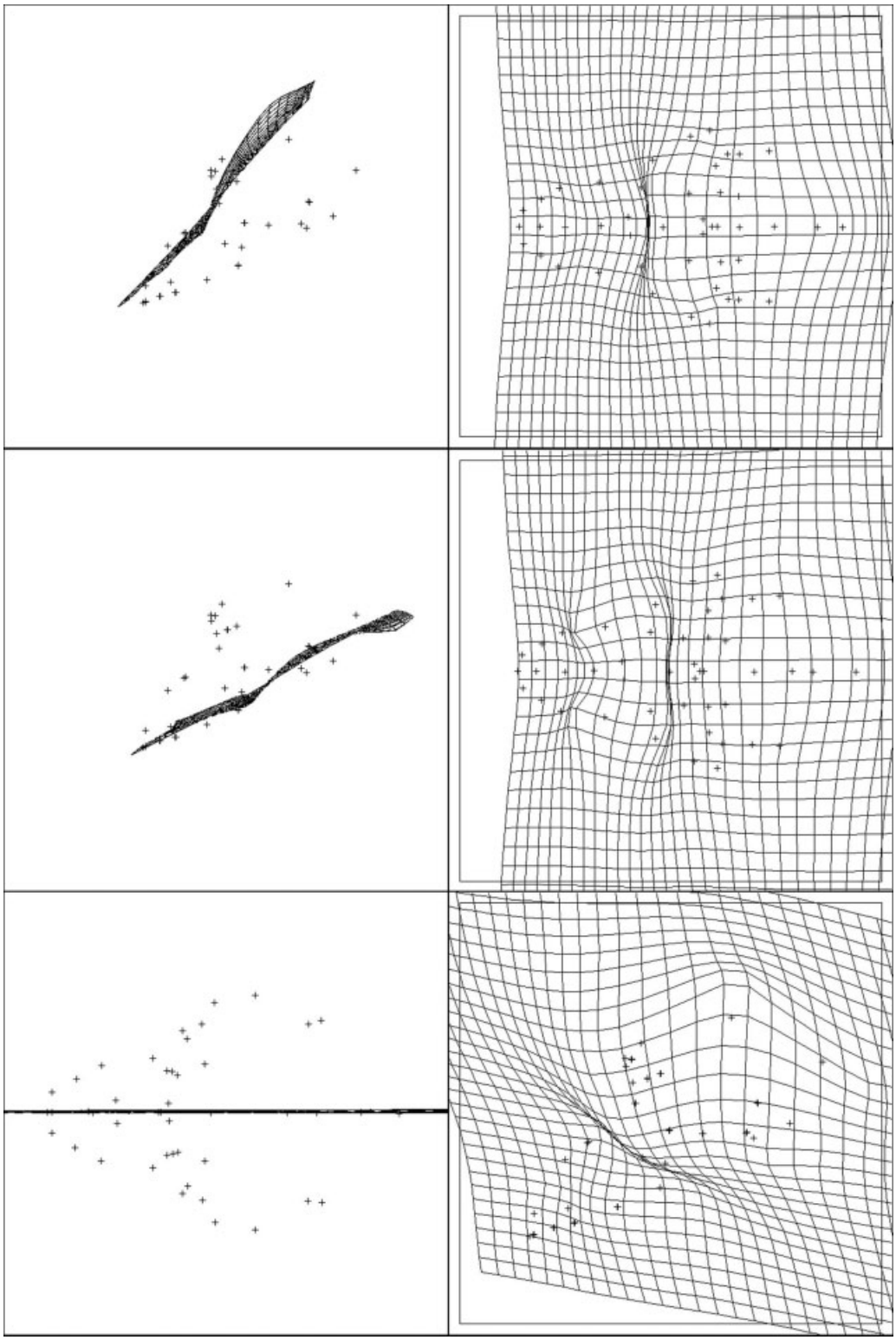

Fig. 5. Three 2D slices of a 3D thin-plate spline, visualized using Edgewarp. The spline is based on deformation of the landmarks, with those of the consensus as the reference and those of the large end of the allometry vector as the target. The left-hand column shows the position of the warped 2D slice on the cranium, which is represented by the consensus landmark configuration. The middle and upper left images are left lateral views of the consensus landmark configuration, and the bottom left image is a dorsal view. Each image in the right-hand column is a perpendicular view of the slice shown in the corresponding left-hand image, but viewed in the plane of the slice. Creases or folds in the deformation grid indicate areas of localized shape change. There is a distinct crease in the region joining the face to the neurocranium, running from the region of the orbits to the back of the palate.

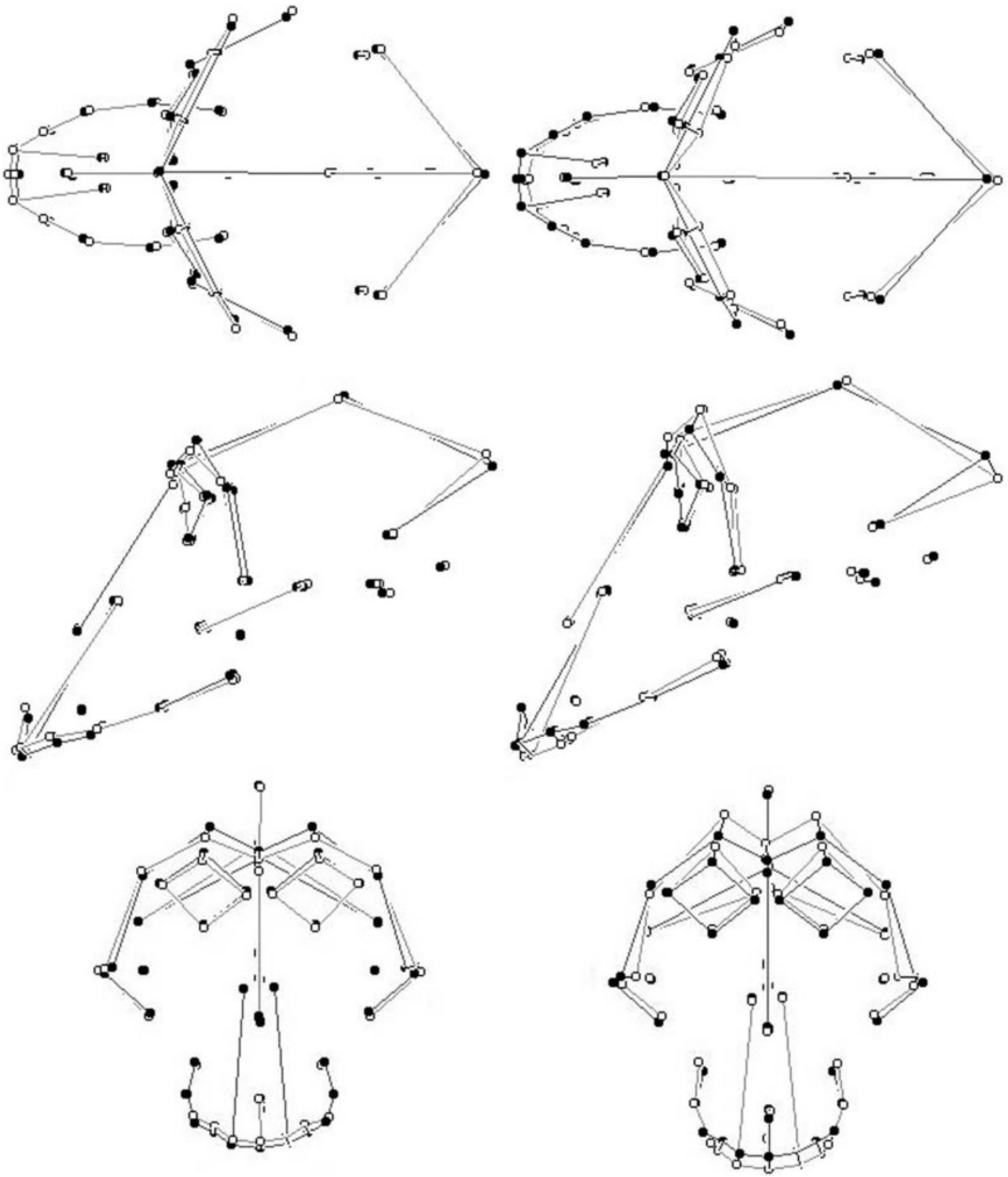

Fig. 6. The mean landmark configuration for males (open circles) adjusted for centroid size vs. the consensus configuration (solid circles) is shown in the left column, and the mean landmark configuration for females (open circles) vs. the consensus configuration (solid circles) is shown in the right column. Views as shown in Figure 4.

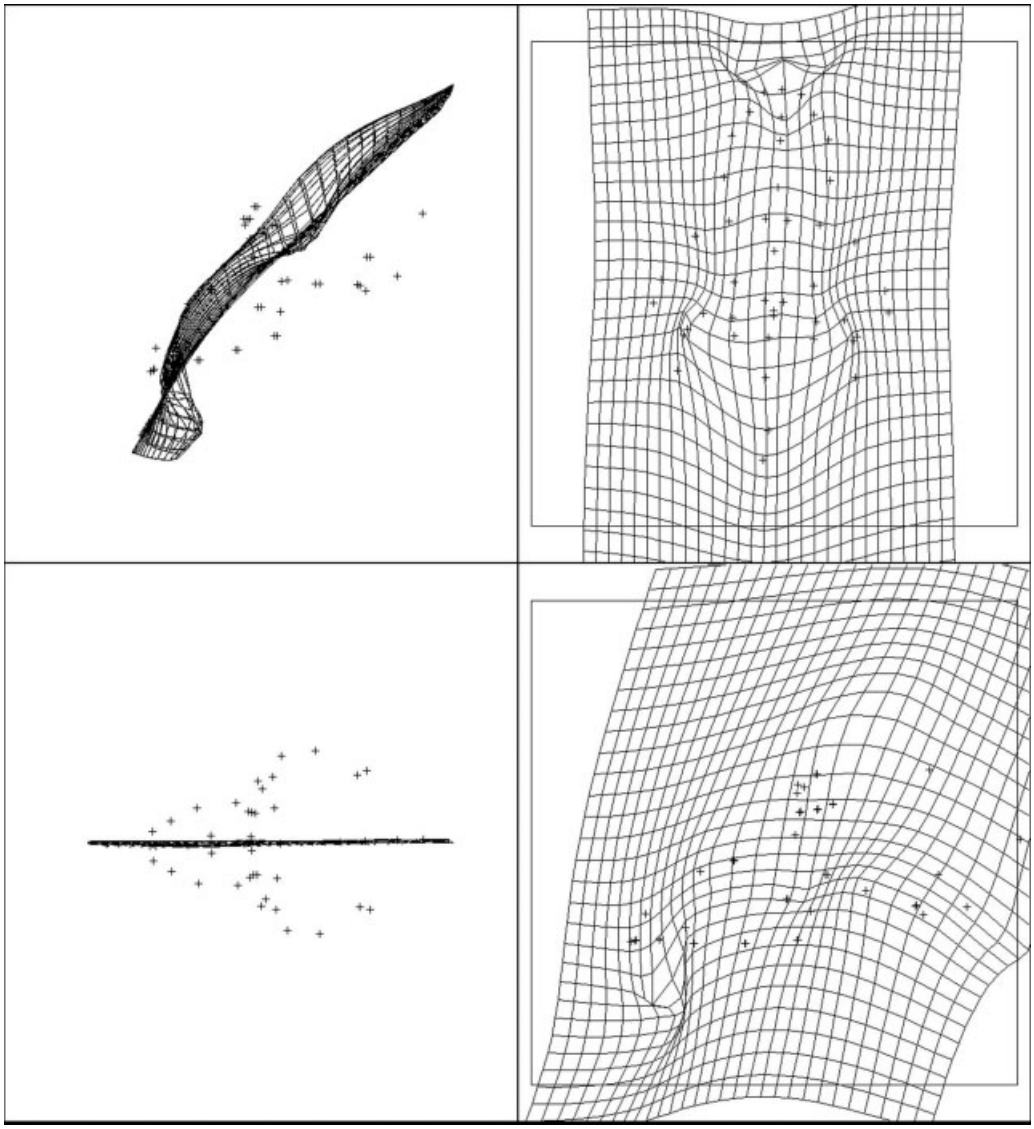

Fig. 7. Two 2D slices of a 3D thin-plate spline are shown. The spline is based on deformation of the landmarks, with those of the size-adjusted male mean as the reference and those of the size-adjusted female mean as the target, extrapolated so one can see the creases. Creases can be observed in the spline in the anterior of the rostrum around the canine, and near the brow area. Panels as described in Figure 5.

clivus of the premaxilla is substantially longer and more vertical, yielding a nasal aperture that is more superiorly oriented. The brow ridges are less arched than those of *Papio*, and the temporal borders of the zygomatic bone slope more inferolaterally (Fig. 10). There are two distinct creases in the splines of the mean size- and sex-adjusted *Theropithecus* and *Papio* configurations (Fig. 11). One is positioned on the dorsal part of the rostrum and is likely related to the short nasals and upturned piriform aperture; the other appears to be related to the projecting glabellar region.

PCA

PCA of tangent space coordinates resulted in the first five PCs accounting for nearly 75% of the total variation (Table 5). PC1 explained 41% of the total variance and summarized many of the shape differences correlated with centroid size (Fig. 12). PC1 makes an angle of 12° (cosine 0.98) with the logged centroid size regression, and has a high correlation with the natural log of centroid size ($R^2 = 0.82$). When shape changes implied by the first eigenvector are applied to the consensus configuration, it agrees very well with the visualization of the size vector described above (Fig. 4). PC1 widely separates males from females within each (sub)species, as would be expected given the large degree of sexual size dimorphism in these species. Since PC1 thus basically tracks overall size, the PC1 scores are not plotted or discussed further. Instead, we present a plot of PC2 and PC3 scores (Fig. 13).

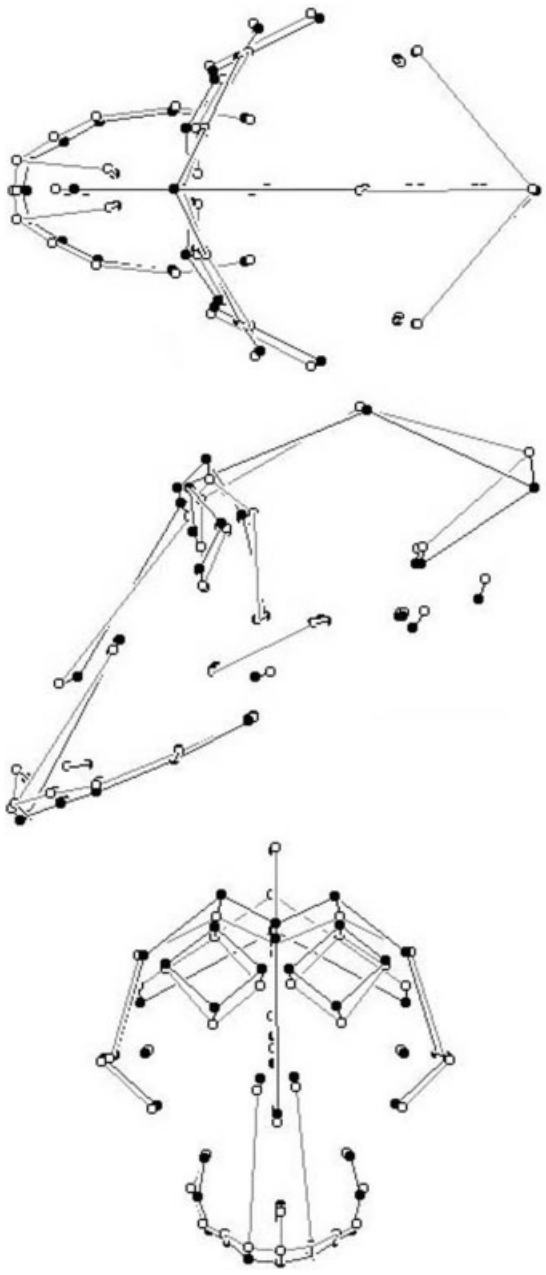

Fig. 8. Mean landmark configurations for *Papio* (open circles) vs. *Mandrillus* (solid circles) adjusted for centroid size and sex. Views as shown in Figure 4.

PC2 separates males of *Mandrillus* from all other specimens, with females of *Mandrillus* being closer in their scores to males of the other genera (Fig. 13). Additionally, PC2 differentiates between males and females in the total sample and within all (sub)species, with the exception of *P.h. papio* and *P.h. hamadryas* (very few female individuals are found in these two taxa). When the shape changes implied by the second eigenvector are visualized, they are essentially similar to the shape differences shown by the mean *Mandrillus* configuration from the consensus (Figs. 8 and 9), and PC2 makes an angle of 28° (cosine 0.88) with the mandrill regression.

PC3 widely separates *Theropithecus* at the positive end of the axis, with *Mandrillus* females at the negative end (Fig. 13). Individuals of *Papio* and male *Mandrillus* are clustered in the center. PC3 also distinguishes the sexes within all (sub)species, except for *P.h. cynocephalus* and *P.h. papio*. Visualization of the shape differences along the third eigenvector yields shape differences consistent with those shown by the mean *Theropithecus* configuration from the consensus (Figs. 10 and 11), and makes an angle of 45° (cosine 0.7) with the *Theropithecus* regression.

PC2 and PC3 widely separate the genera, but higher-order PCs do not clearly separate any of the taxa or sexes. There are differences among means of groups for higher-order PCs, but there is also a substantial amount of overlap. They will not be individually described here.

PCA of the size- and sex-adjusted data set produces a superior separation of the genera compared to that obtained from the unadjusted tangent space coordinates. The first eigenvector accounted for 28.5% of the total variance. The first five eigenvalues of the covariance matrix are listed in Table 5. PC1 separates both species of *Mandrillus* from the other taxa (Fig. 14). Of the other taxa, *P.h. anubis* is closest to the *Mandrillus* species. There is also a small amount of differentiation among *Papio hamadryas* subspecies, with some separation of *P.h. anubis*, *P.h. hamadryas*, and *P.h. papio* from *P.h. cynocephalus*, *P.h. kindae*, and *P.h. ursinus*. When the shape changes implied by PC1 from the size- and sex-adjusted data set are examined, they are quite similar to PC2 from the unadjusted data set, and are essentially the same as those shown by the mean *Mandrillus* configuration compared to the consensus (Figs. 8 and 9). The size- and sex-adjusted PC2 makes an angle of 25° (cosine 0.91) with both the PC1 from the raw tangent space coordinates and the mandrill regression.

PC2 strongly separates *Theropithecus* from the other forms. *M. leucophaeus* is at the opposite extreme to *Theropithecus*, and *Papio* is intermediate, although far closer to *M. leucophaeus*. *M. sphinx* is between *M. leucophaeus* and *Papio* (Fig. 14). When the shape changes implied by PC2 from the size- and sex-adjusted data are visualized, they are similar to those for PC3 from the unadjusted tangent space coordinates and the mean *Theropithecus* configuration (Figs. 10 and 11). The size- and sex-adjusted PC2 makes angles of 32° (cosine 0.85) and 23° (cosine 0.92) with the raw tangent space PC3 and the gelada regression, respectively. The other PCs only poorly separate groups and will not be discussed in detail.

Eigenvalues for within-genus PCAs are collected in Table 5. In the PCA analysis within *Mandrillus*, PC1 accounted for 45% of the total variance. PC1 is largely related to size, and widely separates the sexes. PC2 seems to distinguish the larger males from the other males and females. Most likely these are the males that most strongly display attributes associated with socially dominant males. PC3 accounted for 7% of the total variance, and separated the two species. These numbers compare well with the results from the regression analyses, in which size/sex and species explained 44.6% and 6% of the total variance, respectively. Higher-order PCs had no obvious relationship to sex, taxa, or size. In the PCA within *Papio*, the PC1 was also correlated with size, whereas PC2 largely separated (albeit with substantial overlap) the northern subspecies (*P.h. anubis*, *P.h. hamadryas*, and *P.h. papio*) from the southern ones

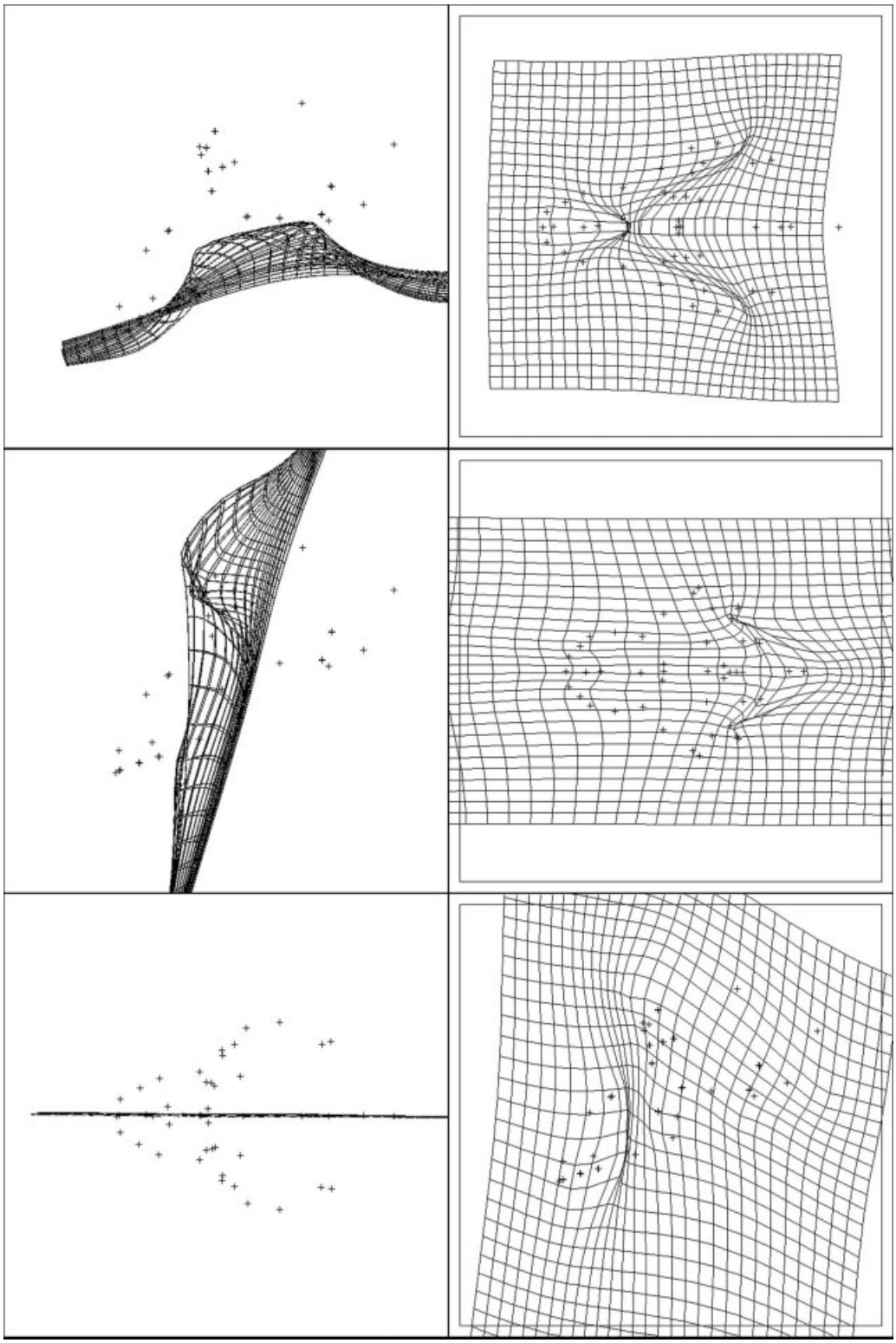

Fig. 9. Three 2D slices of a 3D thin-plate spline are shown. The spline is based on deformation of the landmarks, with those of the size- and sex-adjusted *Papio* mean as the reference and those of the size- and sex-adjusted *Mandrillus* mean as the target. Creases can be observed in the spline at the lateral margins of the neurocranium, and the center of the rostrum. Panels as described in Figure 5.

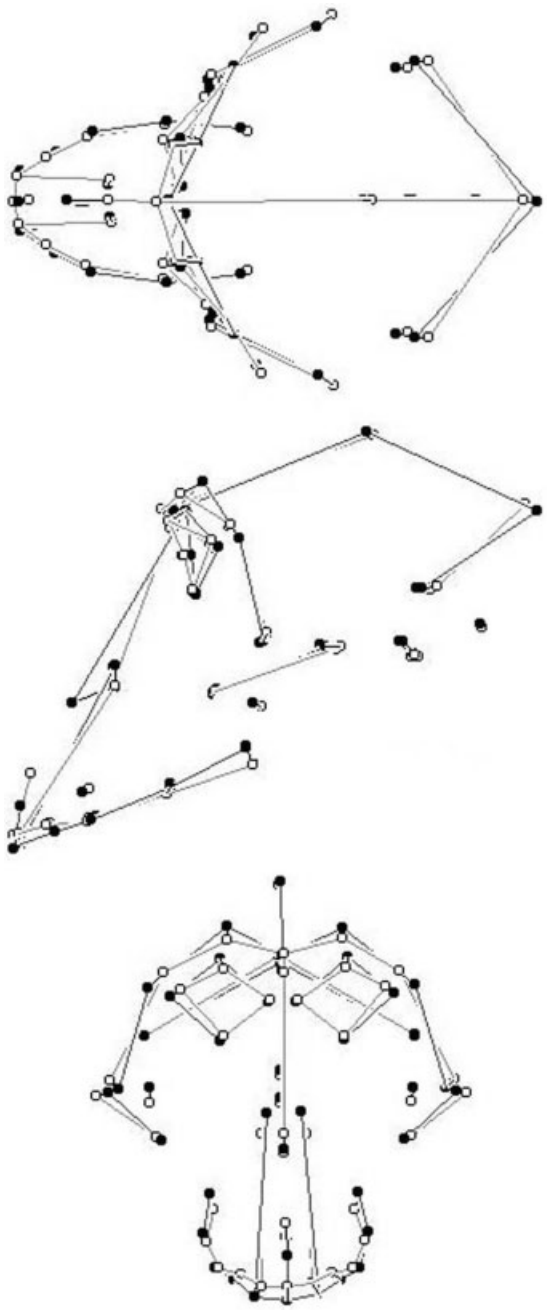

Fig. 10. Mean landmark configurations for *Papio* (open circles) vs. *Theropithecus* (solid circles) adjusted for centroid size and sex. Views as shown in Figure 4.

(*P.h. cynocephalus*, *P.h. kindae*, and *P.h. ursinus*). Within *Theropithecus*, the first PC was related to size, and separated the sexes. Other PCs showed little pattern.

MANCOVA

Scaling patterns within *Mandrillus*, as measured by PCs1-5 on the unadjusted tangent space coordinates, show no significant differences between the sexes or species, nor are there differences in size-adjusted mean shape. Likewise, there is no difference in either scaling pattern or size-adjusted mean shape between males and females of *Theropithecus*. Among the individual subspecies of *P. hamadryas*, however, the situation is more complicated. There is a significant difference in scaling pattern between the sexes ($P = 0.0030$). Among the subspecies, there is a difference in scaling pattern between *P.h. anubis* and *P.h. ursinus* ($P < 0.0001$). There are also differences in size-adjusted mean shape among several of the subspecies (Table 6). For the generic-level comparison, scaling patterns were different between *Mandrillus* and *Papio*, and between *Papio* and *Theropithecus*, but not between *Theropithecus* and *Mandrillus*.

PLS Analysis

The 135 × 2 covariance matrix for size- and sex-adjusted shape coordinates against latitude and longitude in 243 *Papio* revealed a dimension of greatest phylogeography running at about 65° clockwise of the east–west line (the long axis of the continent of Africa). This constructed map coordinate correlates 0.64 with the shape change pattern shown in Figures 15 and 16. Animals from the northwest part of the distribution have flatter, broader crania, while those from the southeastern part have narrower and longer crania. The spline of the consensus landmark configuration to the "northwest end" of this vector shows a crease in the midface related to the flatter crania of baboons from this part of Africa. The geographic distribution of this vector is shown in Figure 17. A second vector correlates 0.58 with the perpendicular map direction, from the Bight of Benin toward the Suez Canal. As this is the short axis of the continent, it explains less shape variation (about 11% of the total phylogeography vs. 89% for the larger component).

Matrix Multiple Regression

Four of the five subspecies contrasts showed an additional component of shape difference as a result of crossing the subspecies barrier. The only contrast without a significant subspecies effect was that between *P.h. cynocephalus* and *P.h. kindae*.

DISCUSSION

Baboon Cranial Shape: Size, Sex, and Taxonomy

As described by previous authors, there is a large component of cranial shape that is correlated with size in baboons (Freedman, 1962, 1963; Cheverud, 1989; Leigh and Cheverud, 1991; Collard and O'Higgins, 2001; Singleton, 2002). The regression analysis shows that shape change correlated with cranial size, or scaling patterns, accounted for just over 35% of Procrustes distance in the total sample (keeping in mind that differences in pure scale were removed by the GPA). Similar values were found within each genus when they were analyzed separately (Table 4). The results of the PCA were similar: PC1 accounted for 41% of total variance in the sample, was highly correlated with centroid size, and made an angle of 12° with the vector from the size regression. There may be some additional factors, such as differences between the sexes, that contribute to PC1, and there may also be aspects of scaling that are not summarized by PC1. One aspect of sexual dimorphism that is probably not allomet-

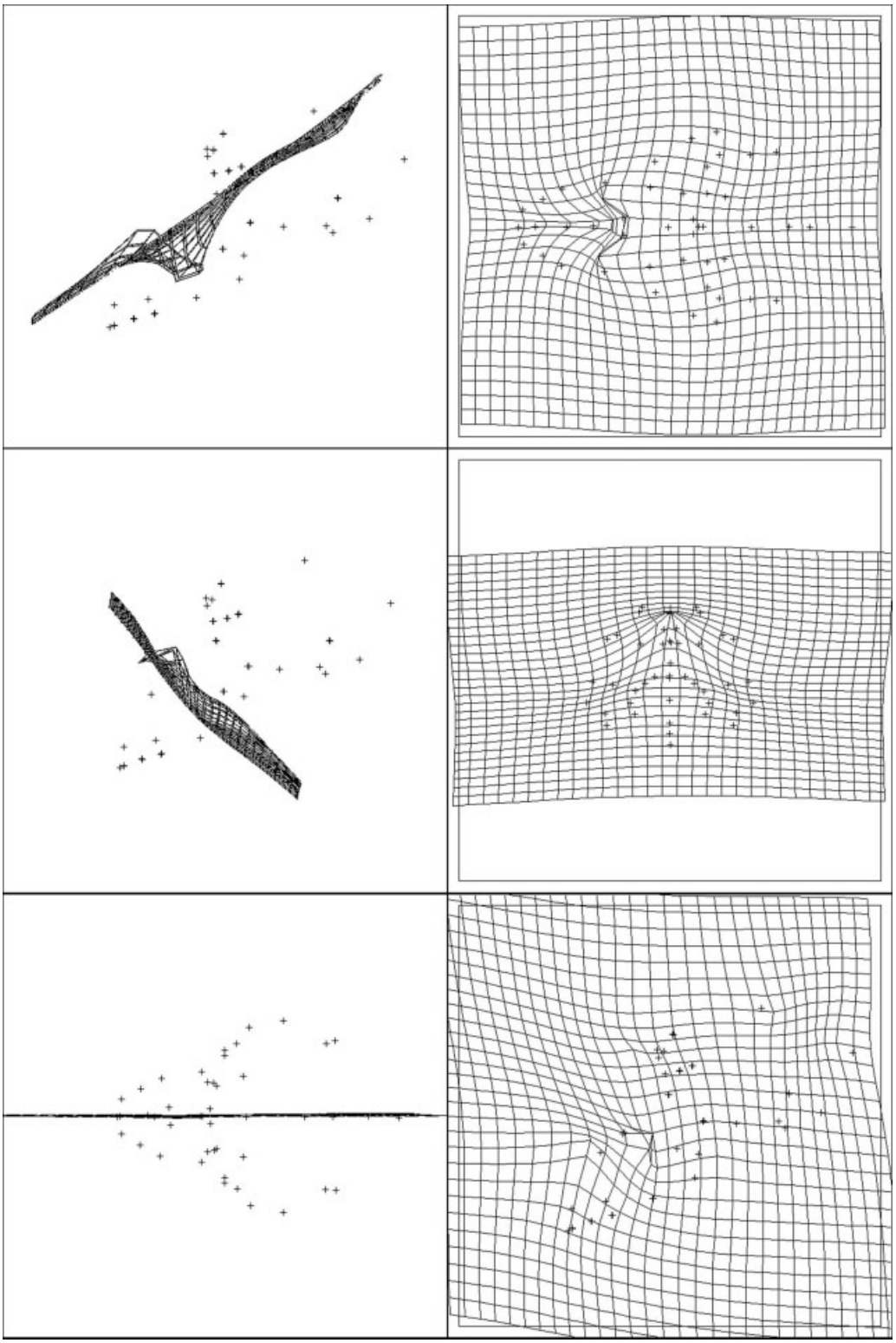

Fig. 11. Three 2D slices of a 3D thin-plate spline are shown. The spline is based on deformation of the landmarks, with those of the size- and sex-adjusted *Papio* mean as the reference and those of the size- and sex-adjusted *Theropithecus* mean as the target. Notice the creases present on the dorsal part of the rostrum and around the glabella. Panels as shown in Figure 5.

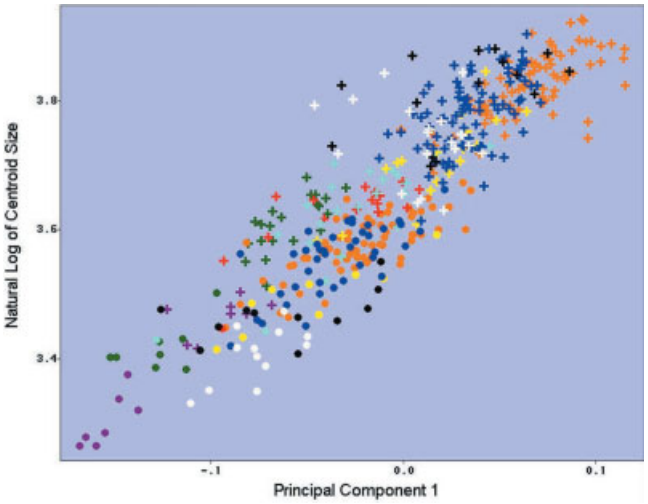

Fig. 12. Bivariate plot with scores of PC1 from the PCA on GPA-aligned coordinates (projected into tangent space) on the X-axis, and the natural log of centroid size on the Y-axis. Plus signs represent males, and circles represent females. Colors are the same as in Figure 1.

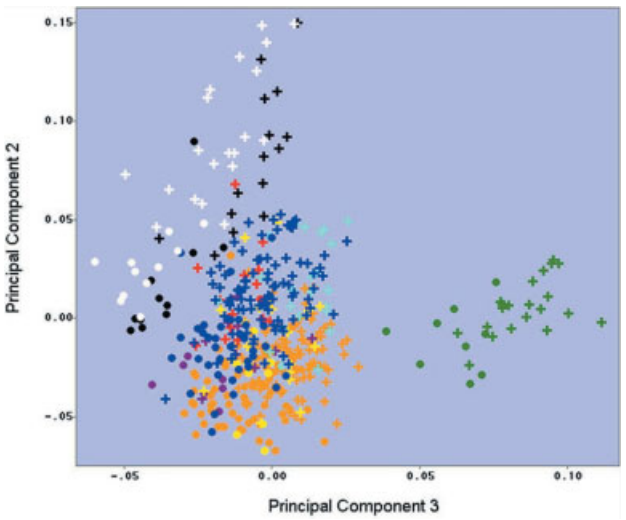

Fig. 13. Scatterplot of scores of PC2 by PC3 from the unadjusted tangent space coordinates for all 452 specimens. Symbols are the same as in Figure 3.

ric, but appears to be included in PC1, is canine size. The scaling vector from the regression analysis shows much smaller differences in canine area, whereas the size-adjusted average male and female configurations show a large difference in this area. Thus, PC1 may be summarizing both scaling and non-allometric components of sexual dimorphism. In any event, when the shape differences implied by PC1 (other than the canine area) are examined, they are essentially the same as those found by the regression analysis of the natural log of centroid size (Fig. 4). The shape changes found in the current study generally match those described in previous analyses (Freedman, 1962, 1963; Cheverud, 1989; Leigh and Cheverud, 1991; Collard and O'Higgins, 2001; Singleton, 2002).

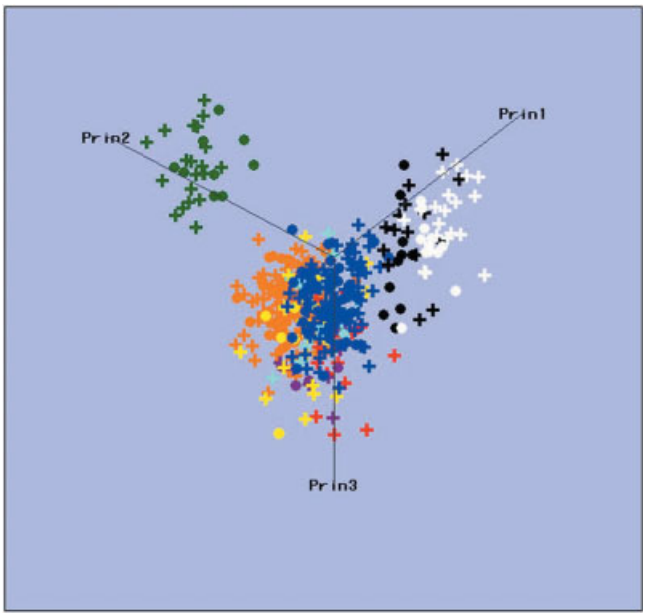

Fig. 14. Three-dimensional plot of individual scores of PC1, PC2, and PC3 for all 452 crania from the size- and sex-adjusted tangent space coordinates, rotated into the orientation that best reveals distinction among the taxa. Symbols are the same as in Figure 3.

As shown by the MANCOVA using PCs1-5 as dependent variables, there are differences in scaling patterns between *Mandrillus* and *Papio*, and between *Papio* and *Theropithecus*, but not between *Theropithecus* and *Mandrillus*. This lack of difference between the latter may be due to the smaller sample sizes of *Theropithecus* and *Mandrillus*. There are clear differences in size-adjusted shape among genera. Within *Mandrillus* there appears to be a difference in scaling pattern between the sexes, but not between the two species. Within *Theropithecus* there is no difference in scaling between the sexes. Within *Papio hamadryas*, there is a difference in scaling pattern between *P.h. anubis* and *P.h. ursinus*, but not among the other subspecies (all of which have much smaller sample sizes). All of the subspecies differ from one another in size-adjusted mean shape, except perhaps for *P.h. kindae* compared to either *P.h. cynocephalus* or *P.h. hamadryas*. However, in spite of these differences among taxa, there is also a large element of the adult scaling pattern that is consistent across taxa. This pattern includes (in larger individuals) a rostrum that is relatively longer compared to the neurocranium and is more klinorhynch in appearance, relatively smaller orbits, a deeper mid-face, and an inion positioned more superiorly relative to the Frankfurt plane.

The sexes are clearly different in all of the taxa examined here. However, the lack of sex-by-species interaction in the MANCOVAs indicates that the overall pattern of sexual dimorphism is similar across all taxa. Most of the shape differences between males and females are clearly related to the fact that they are quite distinct in size, given the strong pattern of allometric scaling. This is reflected in the regression analyses, in that size and sex separately account for 35% and 18% of the Procrustes distance, respectively, but size and sex together account for 39%, and

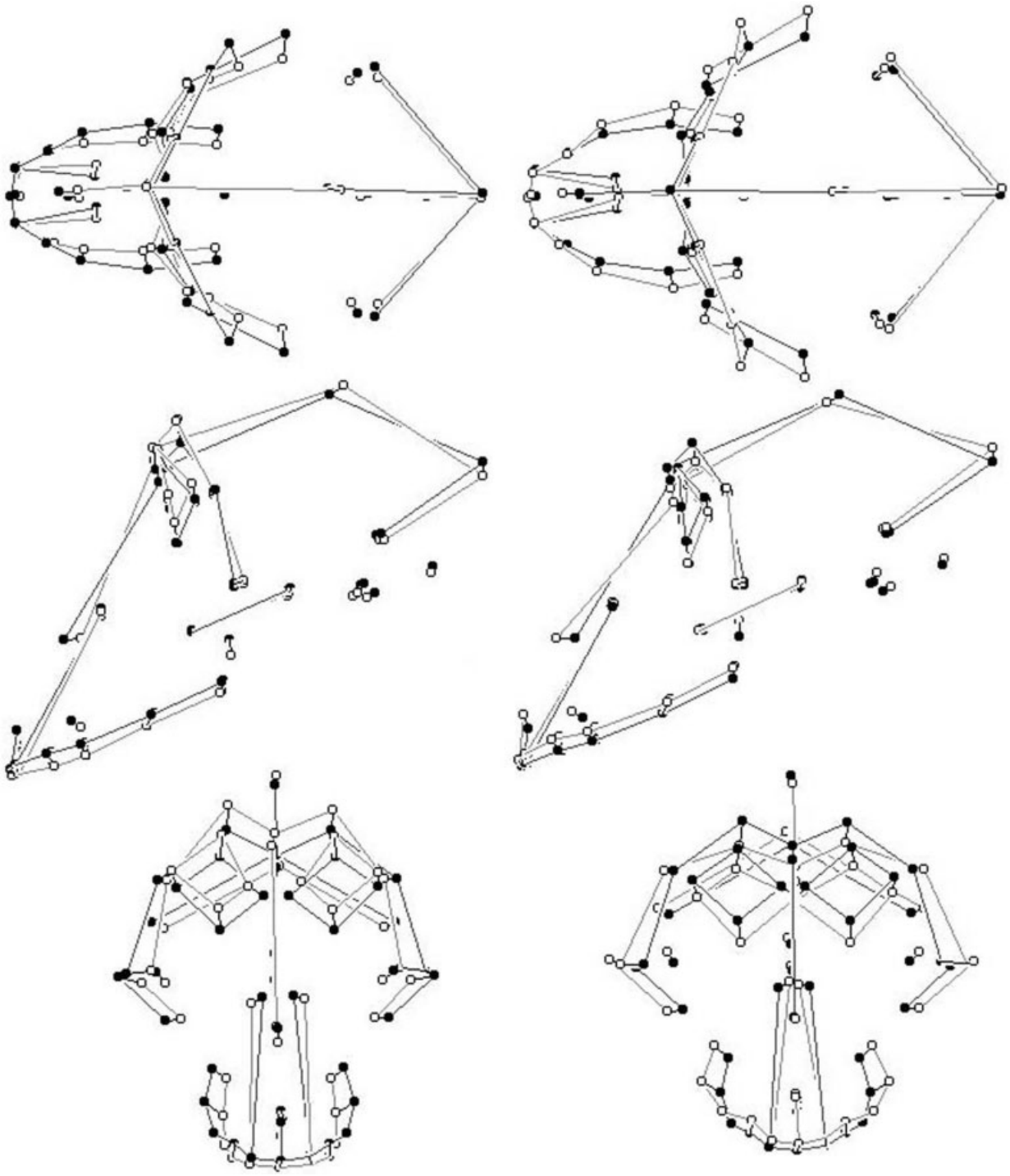

Fig. 15. Visualization of shape changes associated with geography. The left column shows deviations associated with the "northwest" end of the vector (solid circles) from the consensus landmark configuration (empty circles), and the right column shows deviations associated with the "southeast" end (solid circles). Views as shown in Figure 4.

their vectors make an angle of 17° (cosine 0.95). However, some aspects of cranial shape differ between the sexes even after the size difference is adjusted for. These are revealed in examination of the sex vector from the regression analysis. Inspection of the visualizations of the mean forms adjusted to the grand mean centroid size show that the only real areas of difference are in the area of the rostrum around the canine, brow ridge, and inion. Similar

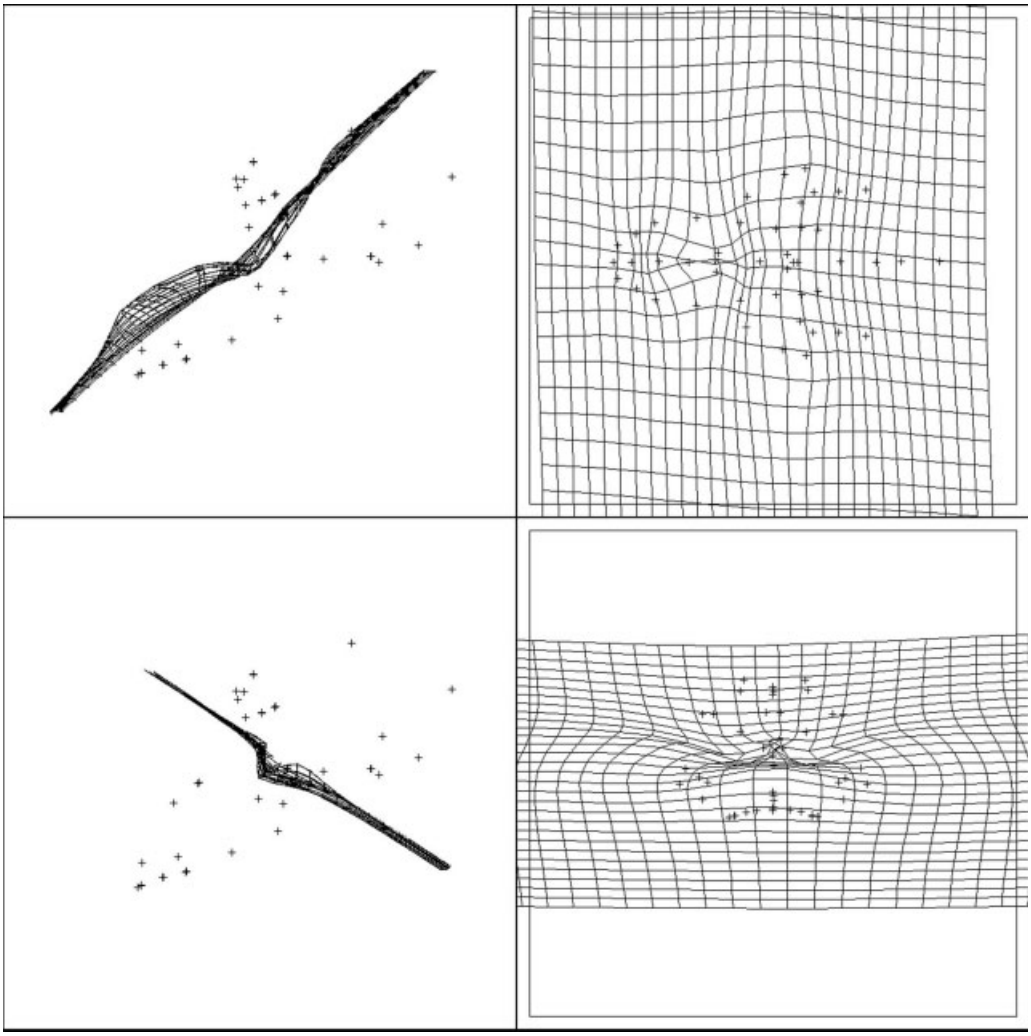

Fig. 16. Two 2D slices of a 3D thin-plate spline are shown. The spline is based on deformation of the landmarks, with those of the consensus as the reference and those of the "northwest" end of the allometry vector as the target. Note the crease running transversely across the midface. Panels are similar to the upper and middle rows of Figure 5.

results were reported in an initial version of this analysis by Marcus et al. (1999), and are concordant with those of several previous analyses of scaling (Freedman, 1962, 1963; Cheverud, 1989; Leigh and Cheverud, 1991).

The three genera are quite distinct in overall cranial shape, as indicated by the Procrustes distances between size- and sex-adjusted species means (Table 6), and by PC1 and PC2 from the size- and sex-adjusted data (Fig. 14; Table 3). The differences among genera are not simply caused by their difference in size, as common scaling effects were removed from this PCA. This can also be seen in the PCA on the unadjusted data set, in that PC2 and PC3 largely separate the genera, and are by definition uncorrelated with PC1, which in turn largely summarizes allometric shape differences. However, it is likely that differences in scaling pattern among some of the genera explain some of the differences in globally adjusted mean shape.

Of the genera examined here, *Theropithecus* has the most morphologically distinctive cranium, as shown by the Procrustes distances between size- and sex-adjusted means (Table 3), and by the large separation in the PCAs on the unadjusted and size- and sex-adjusted tangent space coordinates (Figs. 7 and 8). *Theropithecus* is always at the greatest distance from the other taxa. The distinctive features of *T. gelada*, relative to the other baboons, include a prominent glabellar region and anteriorly projecting brow, which is straighter mediolaterally in frontal view. The alveolar processes are deeper below the M^3, but the incisal portion is relatively higher, giving the alveolar process a more elevated position in comparison to the Frankfurt plane. Finally, the nasal bones are shorter and the profile more convex, yielding a piriform aperture that is more superiorly oriented.

Mandrillus males are obviously distinctive in their cranial morphology, given the presence of the very prominent maxillary ridges and other features related to their facial markings. Their distinctiveness is clear in that PC2 of the unadjusted data clearly separates male drills and man-

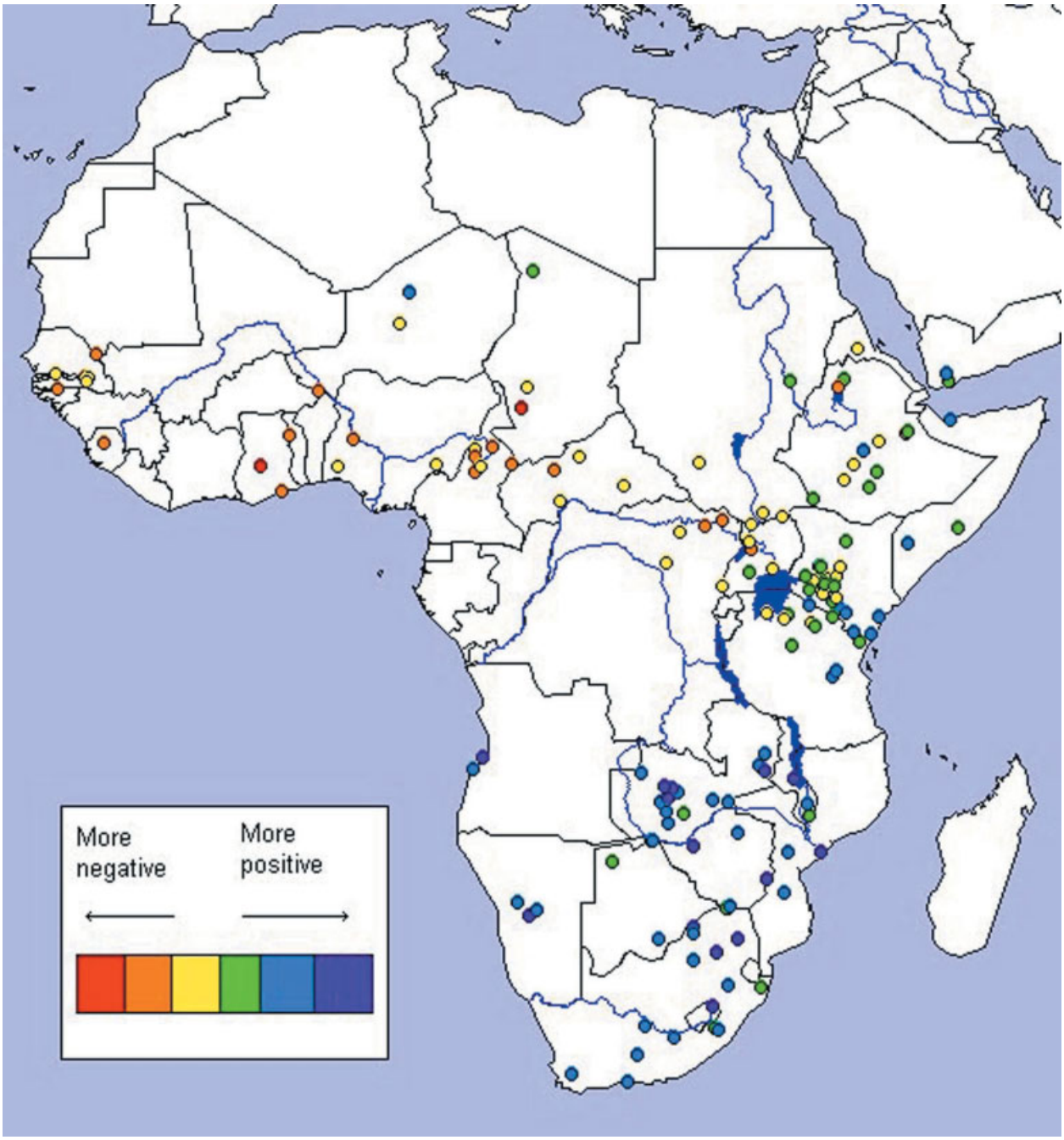

Fig. 17. Individual scores for the first geographic vector plotted on a map of Africa.

drills from *Mandrillus* females and both sexes of the other genera. Both sexes are also quite different from those of the other taxa, as indicated by the fact that PC1 of the size- and sex-adjusted data separated both species and both sexes of *Mandrillus* from the other taxa.

Papio is distinguished from the other genera in having a rostrum that is more klinorhynch in appearance compared to the other two genera. In addition, the nasals are relatively longer than in *Theropithecus*, but generally shorter than in *Mandrillus*. The glabella is more prominent than in *Mandrillus*, but less so than in *Theropithecus*, and the brow ridge of *Papio* is generally higher at the mid-torus relative to the glabella, whereas the others appear to have a brow that is straighter from side to side.

In addition to the generic level, there were significant differences between all of the species and subspecies, both within and among genera. The PCA within *Mandrillus* revealed that while sexual dimorphism accounts for more of the total Procrustes distance, there are significant differences between the two species. *M. leucophaeus* differs

from *M. sphinx* in being more extreme for all of the features that distinguish *Mandrillus* from the other genera.

The subspecies of *Papio* are also distinct from one another in patterns of overall cranial shape, in aspects that are not correlated with size (i.e., non-allometric). The PCA within *Papio* on the size- and sex-adjusted data separates the subspecies, with overlap. In particular, the northern forms (*P.h. papio*, *P.h. hamadryas*, and *P.h. anubis*) are separated from the southern forms (*P.h. cynocephalus, P.h. kindae*, and *P.h. ursinus*).

Phylogeography of *Papio* Baboons

The PLS analysis of size- and sex-adjusted *Papio* PC1-5 with locality coordinates shows a strongly clinal pattern (Fig. 17), with geography explaining a large component of the Procrustes distance within *Papio*. This pattern is reinforced by the Procrustes distances of the size- and sex-adjusted (sub)species means, and a minimum spanning tree of these links geographic neighbors (Fig. 18). However, as demonstrated by the matrix multiple regression of shape on geographic distance, there is a significant additional component of Procrustes distance accounted for by differences in subspecies, except between *P.h. cynocephalus* and *P.h. kindae.* Thus the baboons show a stepped cline in cranial morphology from north to south, with northern varieties having broader crania and rostra that are less flexed compared to those of southern African baboons, which have narrower crania and rostra that are more inferiorly flexed (i.e., relatively klinorhynch).

This strongly geographic patterning of cranial differences argues for the various forms of *Papio* baboons being ranked as subspecies and not as full species. If the different forms were indeed full species, in the sense of the biological species concept, one would expect a less clinal pattern of similarities, with character displacement across contact zones. On the other hand, if nearest geographic neighbors speciated more recently than those that are further apart, one might find a similar geographic pattern among full species. Similarly, if there were a clear functional-adaptive significance to the differences in cranial shape that correlated with some ecological gradient across Africa, then such a pattern as we observed might again be produced among distinct, but closely related species.

However, when other evidence is considered along with the pattern of cranial variation presented here, a consistent pattern appears to emerge. At least two zones of interbreeding between *Papio* baboons have been directly observed: between *P.h. hamadryas* (which is distinct from other baboon varieties in its social behavior, pelage, and facial coloration) and *P.h. anubis* in Ethiopia; and between *P.h. anubis* and *P.h. cynocephalus* in Tanzania (Jolly, 1993). Studies of additional contact regions between pairs of *Papio* populations might further support the current hypothesis of genetic continuity. In addition, molecular data that are currently being analyzed reveal a similar geographic pattern of variation (Newman et al., 2000; Wildman, 2000; Newman et al., in press). When these three lines of evidence are combined, it appears that the taxonomy of *Papio* is best summarized as a series of allopatric subspecies under the biological species concept.

Why is it important to know whether the populations of one primate genus are best ranked as a species or subspecies? Groves (2001, pgs. 237–238) reported that he had modified his own opinion of baboon systematics several times in the past decades, but that he was "confident, however, that the five species traditionally recognized are genuinely diagnosable entities," and he clearly diagnosed them. Under a phylogenetic species concept, such diagnosability indeed implies species rank, and Groves further reported that Jolly (1993) had ultimately accepted a "phylogenetic subspecies" concept roughly equivalent to our own interpretation. Although the long history of countercharges among proponents of alternative species concepts is beyond the scope of this report, it is clear that problems arise when the phylogenetic species concept is applied to complex groups of populations. As Lee (2003) recently argued, it is still only the biological species concept that makes the species a distinctive level of hierarchical organization, and interbreeding is the only species criterion that allows a relatively narrow and objective discrimination of the species boundary. For these reasons, the current authors prefer the biological species concept. Thus, the question of baboon systematics is a meaningful one, and we suggest that the approach presented here may be more objective than others, as well as widely applicable.

Some interesting patterns of phenetic difference are also worthy of note here. It is important to keep in mind that the phenetic distance (as measured by the landmark set used here) between some of the *Papio hamadryas* subspecies is greater than the distance between the two species of *Mandrillus*. Thus, it is not the magnitude of the differences between the subspecies of *Papio* that argues for subspecific rank, but the *pattern* of those differences, and their relationship to geography. Additionally, the phenetic distance between *Theropithecus* and *Papio* is greater than that between *Mandrillus* and *Papio*. This pattern is the opposite of their phylogenetic relationship, as inferred from genetic data. Once again, the magnitude of the difference should not be used to infer taxonomic status. What can be determined is that *Theropithecus* has evolved a more distinctive cranium compared to the other two genera in a relatively short period of time, and that the rate of morphological evolution has been far from homogeneous in baboons.

Next Steps

This analysis was based solely on the study of landmarks and their geometry, and on extant populations of the large African papionins. Two extensions of this study are in progress, involving the incorporation of semi-landmarks interpolated along space curves, and the inclusion of samples from extinct taxa. The study of space curves allows a much greater range of complex morphology to be considered, compared to simple landmark analysis (Bookstein et al., 1999; Delson et al., 2001; Singleton, 2002). Techniques such as the "sliding" of semi-landmarks improve the application of Procrustes analysis to curvilinear data. The addition of distinct morphologies represented by fossil representatives of the extant *Papio* and *Theropithecus*, as well as entirely extinct genera or subgenera such as *Parapapio*, *Pliopapio*, and *Dinopithecus*, provides a much greater range of structure for analysis, and enables one to infer phylogenetic relationships that are not amenable to molecular genetic study.

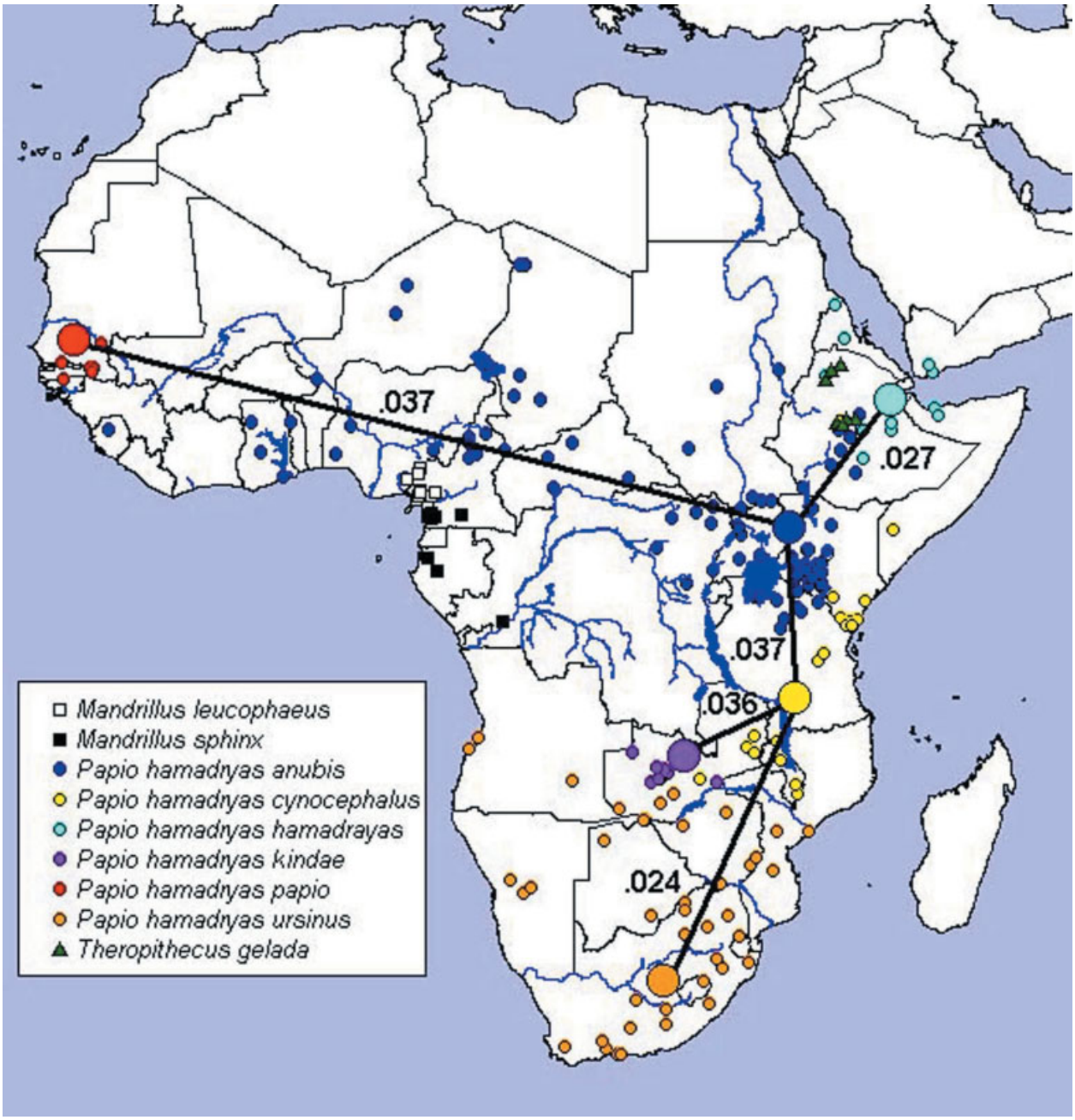

Fig. 18. Map of Africa with localities of analyzed savannah baboon specimens and a superimposed minimum spanning tree based on the Procrustes distances between size- and sex-adjusted subspecies means (data in Table 3).

ACKNOWLEDGMENTS

We thank the many curators and staffs of the institutions who provided access to specimens in their care, and much assistance: Dr. Kevin Kuykendal, Anatomy Department, University of the Witwatersrand, Johannesburg; Dr. Ina Plug, Transvaal Museum, Pretoria; Dr. Paula Jenkins, British Museum (Natural History), London; the staff of the Powell-Cotton Museum, Birchington; Jacques Repéperant and Francis Renoult, Musée National d'Histoire Naturelle, Paris; Prof. Wolfgang Maier, Lehrstuhl für Spezielle Zoologie, Universität Tübingen; Dr. G. Storch, Forschungsinstitut Senkenberg, Frankfurt; Dr. Richard Thorington and Linda Gordon, National Museum of Natural History, Smithsonian Institution, Washington, D.C.; and Drs. Chris Norris, Ross MacPhee, Nancy Simmons, and Robert Randall, American Museum of Natural

History, New York. Drs. Jim Rohlf and Michelle Singleton and two anonymous reviewers provided useful comments on various versions of this project. This is NYCEP Morphometrics contribution number 5.

LITERATURE CITED

Albrecht GH. 1978. The craniofacial morphology of the Sulawesi macaques. Multivariate approaches to biological problems. Contrib Primatol 13:1–151.

Bookstein FL. 1996. Combining the tools of geometric morphometrics. In: Marcus LF, Corti M, Loy A, Naylor GJP, Slice DE, editors. Advances in morphometrics. New York: Plenum Press. p 131–151.

Bookstein FL, Schäfer K, Prossinger H, Seidler H, Fieder M, Stringer C, Weber G, Arsuaga J-L, Slice DE, Rohlf FJ, Recheis W, Mariam J, Marcus LF. 1999. Comparing frontal cranial profiles in archaic and modern *Homo* by morphometric analysis. Anat Rec (New Anat) 257:217–224.

Bookstein FL. 2000. Creases as local features of deformation grids. Med Image Anal 4:93–110.

Bookstein FL. 2002. Creases as morphometric characters. In: MacLeod N, Forey P, editors. Morphology, shape, and phylogeny. Systematic Association Special Volume Series 64. London: Taylor and Francis. p 139–174.

Cheverud JM. 1989. A comparative analysis of morphological variation patterns in the papionins. Evolution 43:1737–1747.

Collard M, O'Higgins P. 2001. Ontogeny and homoplasy in the papionin face. Evol Dev 3:322–331.

Delson E, Dean D. 1993. Are *Papio baringensis* R. Leakey, 1969, and *P. quadratirostris* Iwamoto, 1982, species of *Papio* or *Theropithecus*? In: Jablonski NG, editor. *Theropithecus*: the rise and fall of a primate genus. Cambridge: Cambridge University Press. p 125–156.

Delson E, Terranova CJ, Jungers WL, Sargis EJ, Jablonski NG, Dechow PC. 2000. Body mass in Cercopithecidae (Primates, Mammalia): estimation and scaling in extinct and extant taxa. Am Mus Nat Hist Anthropol Pap 83:1–159.

Delson E, Harvati K, Reddy D, Marcus LF, Mowbray K, Sawyer GJ, Jacob T, Márquez S. 2001. The Sambungmacan 3 Homo erectus calvaria: a comparative morphometric and morphological analysis. Anat Rec 262:360–377.

DeVore I, Washburn SL. 1963. Baboon ecology and human evolution. In: Howell FC, Bourlière F, editors. African ecology and human evolution. New York: Walter de Gruyter. p 335–367.

Disotell TR. 1994. Generic level relationships of the Papionini (Cercopithecoidea). Am J Phys Anthropol 94:47–57.

Dryden IL, Mardia KV. 1998. Statistical shape analysis. John Wiley: New York. 376 p.

Eck GG, Jablonski N. 1987. The skull of *Theropithecus brumpti* compared with those of other species of the genus *Theropithecus*. Cahiers de paléontologie. Travaux de paléontologie est-africaine. Les faunes Plio-Pléistocènes de la Vallée de l'Omo (Éthiopie). Vol. 3, Cercopithecidae de la Formation de Shungura. Paris: Éditions du C. N. R. S. p 11–122.

Enlow DH. 1975. Handbook of facial growth. Toronto: W.B. Saunders.

Fleagle JG. 1999. Primate adaptation and evolution. 2nd ed. San Diego: Academic Press. 596 p.

Fleagle JG, McGraw S. 1999. Skeletal and dental morphology supports diphyletic origin of baboons and mandrills. Proc Natl Acad Sci USA 96:1157–1161.

Fleagle JG, McGraw S. 2002. Skeletal and dental morphology of African papionins: unmasking a cryptic clade. J Hum Evol 42:267–292.

Freedman L. 1962. Growth of muzzle length relative to calvaria length in *Papio*. Growth 26:117–128.

Freedman L. 1963. A biometric study of *Papio cynocephalus* skulls from northern Rhodesia and Nyasaland. J Mammal 44:24–43.

Groves CP. 1989. A theory of human and primate evolution. Oxford: Oxford University Press. 392 p.

Groves CP. 2001. Primate taxonomy. Washington, DC: Smithsonian Institution Press. 350 p.

Harris EE, Disotell TR. 1998. Nuclear gene trees and the phylogenetic relationships of the mangabeys (Primates: Papionini). Mol Biol Evol 15:892–900.

Harris EE. 2000. Molecular systematics of the Old World Monkey tribe Papionini: analysis of the total available genetic sequences. J Hum Evol 38:235–256.

Hewett-Emmett D, Cook CN, Barnicot NA. 1976. Old World monkey hemoglobins: deciphering phylogeny from complex patterns of molecular evolution. In: Goodman M, Tashian RE, editors. Molecular anthropology. Genes and proteins in the evolutionary ascent of the Primates. New York: Plenum Press. p 257–275.

Hill WCO. 1970. Primates: comparative anatomy and taxonomy, VIII Cynopithecidae: *Papio*, *Mandrillus*, and *Theropithecus*. Edinburgh: Edinburgh University Press. 680 p.

Iwamoto T. 1993. The ecology of *Theropithecus gelada*. In: Jablonski NG, editor. *Theropithecus*: the rise and fall of a primate genus. Cambridge: Cambridge University Press. p 441–452.

Jolly CJ. 1967. The fossil history of the baboons. In: Vagtborg H, editor. The baboon in medical research, II. Austin, TX: University of Texas Press. p 23–50.

Jolly CJ. 1970. The large African monkeys as an adaptive array. In: Napier JR, Napier PH, editors. Old World monkeys—evolution, systematics, and behavior. New York: Academic Press. p 141–174.

Jolly CJ. 1972. The classification and natural history of *Theropithecus* (*Simopithecus*) (Andrews, 1916), baboons of the African Plio-Pleistocene. Bull Br Mus (Nat Hist) Geol 22:1–122.

Jolly CJ, Brett FL. 1973. Genetic markers and baboon biology. J Med Primatol 2:85–99.

Jolly CJ. 1993. Species, subspecies and baboon systematics. In: Kimbel WH, Martin LB, editors. Species, species concepts, and primate evolution. New York: Plenum Press. p 67–107.

Jolly CJ. 2001. A proper study for mankind: analogies from the papionin monkeys and their implications for human evolution. Yearb Phys Anthropol 44:177–204.

Lee MSY. 2003. Species concepts and species reality: salvaging a Linnaean rank. J Evol Biol 16:179–188.

Leigh SR, Cheverud JM. 1991. Sexual dimorphism in the baboon facial skeleton. Am J Phys Anthropol 84:193–208.

Manly BFJ. 1994. Multivariate statistical methods, a primer. 2nd ed. Boca Raton, FL: Chapman & Hall. 323 p.

Marcus et al. 1997. http://research.amnh.org/nycep/microscribe_vs_polhemus.html

Marcus LF, Frost SR, Bookstein FS, Reddy DP, Delson E. 1999. Comparison of landmarks among *Papio* skulls, with extension of Procrustes methods to ridge curves. Am J Phys Anthropol 108:190.

Napier PH. 1981. Catalog of primates in the British Museum (Natural History) and elsewhere in the British Isles, Part II: family Cercopithecinae, subfamily Cercopithecinae. London: British Museum (Natural History). 203 p.

Neff NA, Marcus LF. 1980. A survey of multivariate methods for systematics. New York: American Museum of Natural History. 243 p.

Newman TK, Wildman DE, Bergman TJ, Rogers J. 2000. An expanded mtDNA phylogeny and its implications for gene flow and biogeography in baboons. Am J Phys Anthropol S30;237.

Newman TK, Jolly CJ, Rogers J. Mitochondrial phylogeny and systematics of baboons. Am J Phys Anthropol (in press).

Oates JF. 1996. African primates: status survey and conservation action plan. Revised edition. Gland: IUCN.

O'Higgins P, Jones N. 1998. Facial growth in *Cercocebus torquatus*: an application of three-dimensional geometric morphometric techniques to the study of morphological variation. J Anat 193: 251–272.

Ravosa MJ, Profant LP. 2000. Evolutionary morphology of the skull in Old World monkeys. In: Whitehead PF, Jolly CJ, editors. Old World monkeys. New York: Cambridge University Press. p 237–268.

Rohlf FJ, Slice DE. 1990. Extensions of the Procrustes method for the optimal superimposition of landmarks. Syst Zool 39:40–59.

Rohlf FJ. 1999. Shape statistics: Procrustes superimpositions and tangent spaces. J Class 16:197–223.

Rohlf FJ, Corti M. 2000. Use of two-block partial least-squares to study covariation in shape. Syst Biol 49:740–753.

Rohlf FJ. 2002. Tps Small, version 1.19. Stony Brook, NY: State University of New York.

Sarich VM, Cronin JE. 1976. Molecular systematics of the primates. In: Goodman M, Tashian RE, editors. Molecular anthropology. Genes and proteins in the evolutionary ascent of the Primates. New York: Plenum Press. p 141–170.

Sarmiento E. 1999. Current problems with *Papio* taxonomies. Afr Primates 3:48–52.

Singleton AM. 2002. Patterns of cranial shape variation in the Papionini (Primates: Cercopithecinae). J Hum Evol 42:547–578.

Slice DE, Bookstein FL, Marcus LF, Rohlf FJ. 1996. Appendix I. A glossary of geometric morphometrics. In: Marcus LF, Corti M, Loy A, Naylor GJP, Slice DE, editors. Advances in morphometrics. New York: Plenum Press. p 531–551.

Strasser E, Delson E. 1987. Cladistic analysis of cercopithecid relationships. J Hum Evol 16:81–99.

Szalay FS, Delson E. 1979. Evolutionary history of the Primates. San Diego: Academic Press. 580 p.

Thorington RW, Groves CP. 1970. An annotated classification of the Cercopithecoidea. In: Napier JR, Napier PH, editors. Old World monkeys—evolution, systematics, and behavior. New York: Academic Press. p 629–648.

Vogel C. 1968. The phylogenetic evaluation of some characters and some morphological trends in the evolution of the skull in catarrhine primates. In: Chiarelli AB, editor. Taxonomy and phylogeny of Old World primates with references to the origins of man. Torino: Rosenberg and Sellier. p 21–55.

White TD. 2000. Human osteology. 2nd ed. San Diego: Academic Press. 563 p.

Wildman DE. 2000. Mammalian zoogeography of the Arabian peninsula and horn of Africa with a focus on the cladistic phylogeography of hamadryas baboons (primates: *Papio hamadryas*). Ph.D. thesis, New York University, New York.

Zuckerman S. 1926. Growth changes in the skull of the baboon, *Papio porcarius*. Proc Zool Soc Lond 55:843–873.